

**University of São Paulo**  
**Institute of Geosciences**  
**Graduate Program in Geosciences (Geochemistry and Geotectonics)**

Tainã Marcos Lima Pinho

**Basin-wide paleoceanographic changes in the upper South Atlantic during  
Heinrich Stadials over the last 70 kyr**

São Paulo

2021

TAINÃ MARCOS LIMA PINHO

**Basin-wide paleoceanographic changes in the upper South Atlantic during  
Heinrich Stadials over the last 70 kyr**

MSc. Dissertation presented to the Graduate  
Program in Geosciences (Geochemistry and  
Geotectonics) at the Institute of Geosciences,  
University of São Paulo to obtain the degree of  
Master of Science

Area of concentration:

Geochemistry of Exogenous Processes

Supervisor: Prof. Dr. Cristiano Mazur Chiessi

São Paulo

2021

Autorizo a reprodução e divulgação total ou parcial deste trabalho, por qualquer meio  
convencional ou eletrônico, para fins de estudo e pesquisa, desde que citada a fonte.

**University of São Paulo**  
**Institute of Geosciences**  
**Graduate Program in Geosciences (Geochemistry and Geotectonics)**

**Basin-wide paleoceanographic changes in the upper South Atlantic during  
Heinrich Stadials over the last 70 kyr**

**TAINÃ MARCOS LIMA PINHO**

Supervisor: Prof. Dr. Cristiano Mazur Chiessi

Master dissertation

**Nº 873**

**COMISSÃO JULGADORA**

Dr. Cristiano Mazur Chiessi

Dr. Thiago Pereira dos Santos

Dra. María Alejandra Gómez Pivel

São Paulo

2021

## Acknowledgments

I would like to thank my advisor, Prof. Dr. Cristiano Mazur Chiessi for his outstanding mentorship and for all the opportunities he provided to me during the time I was a Master's student. His thorough support was certainly essential to bring this dissertation to a higher level. I will always be grateful for our partnership over these years, and hope that the partnership will continue.

I would also like to thank my colleagues at the Paleoceanography and Paleoclimatology Laboratory (P2L) at the School of Arts, Sciences and Humanities, and the Institute of Geosciences, University of São Paulo for their insightful discussions in our meetings as well as during the laboratory work. Specially, I would like to thank Dr. Marília Campos for our long discussions and hardworking together, Dr. Stefano Crivellari for all his technical support by the period of my geochemical analysis.

A particular thanks goes to Dr. Rodrigo da Costa Portilho-Ramos for our uncountable and constructive discussions personally and remotely during the last five years. I would also like to thank him for teaching me how to identify the planktonic foraminifera shells and all the friendly and broadly conversations.

I am grateful to the infrastructure of the University of São Paulo that made possible my Master's degree. I thank FAPESP for the MSc. Scholarship (Grant 2019/10642-6) as well as for other projects that partially funded this study (Grants 2018/15123-4 and 2019/24349-9). The support from CAPES (Grants 564/2015, 88887.156152/2017-00, 88881.161151/2017-01 and 88881.313535/2019-01), CNPq (Grants 302607/2016-1 and 312458/2020-7) and the Alexander von Humboldt Foundation is also acknowledged.

Finally, I thank my wife for all her support either in good and bad moments and for her unconditional careful, which I am immensely grateful. Sharing my life with you is such a privilege.

## Resumo

Pinho, T. M. L., **Mudanças paleoceanográficas em larga escala na superfície do Atlântico Sul durante os Heinrich Stadials para os últimos 70 kyr.** Dissertação (Mestrado) – São Paulo, Instituto de Geociências, Universidade de São Paulo, 2021. 98 pp

Reconstruções paleoceanográficas em regiões-chave do Atlântico Sul são importantes para entender seu papel na variabilidade climática global. No entanto, os dados disponíveis carecem de registros contínuos que abrangem todos os eventos de mudanças climáticas abruptas em escala milenar do último período glacial. Apresentamos aqui um conjunto de registros composto por dados micropaleontológicos e isotópicos obtidos em foraminíferos planctônicos de um testemunho sedimentar marinho coletado na porção oeste do Atlântico Sul tropical no limite norte do Giro Subtropical do Atlântico Sul (GSAS) cobrindo os últimos 70 kyr. Nós comparamos a abundância de *Globorotalia truncatulinodes* do nosso testemunho sedimentar com um registro publicado anteriormente da mesma espécie oriundo do limite sul do GSAS para reconstituir as flutuações meridionais do GSAS. Nossos resultados indicam deslocamentos para o sul do GSAS durante os Heinrich Stadials (HS) 6-4 e HS1, e uma contração do GSAS durante os HS3 e HS2. Durante os HS6-4 e HS1, os deslocamentos do GSAS para o sul provavelmente aumentaram a transferência de calor para o Oceano Austral, fortalecendo a ressurgência de águas profundas e a liberação de CO<sub>2</sub> para a atmosfera. Isso é de importância primordial, uma vez que o deslocamento em curso do GSAS em direção ao polo pode aumentar ainda mais a liberação de CO<sub>2</sub> oceânico. Neste trabalho propomos um novo indicador para o deslocamento meridional do GSAS em escala milenar baseado na abundância relativa de *G. truncatulinoides*. Além da abundância de *G. truncatulinoides*, também analisamos a composição dos isótopos estáveis de carbono ( $\delta^{13}\text{C}$ ) dessa espécie. Nossa registro de  $\delta^{13}\text{C}$  da termoclina, juntamente com dados similares do SE-Atlântico Sul, mostram excursões negativas durante a maioria dos HS. Além disso, nosso registro de  $\delta^{13}\text{C}$  da termoclina exibe maiores excursões negativas de  $\delta^{13}\text{C}$  em comparação com as excursões do registro do SE-Atlântico Sul. Nós sugerimos que as causas de tais excursões são o fortalecimento da ressurgência e ocorrência de uma bomba biológica ineficiente no Oceano Austral. Além disso, o sinal de  $\delta^{13}\text{C}$  que deixou o Oceano Austral ainda sofreu diminuição pelo efeito do envelhecimento da massa d'água que aumentou o conteúdo de carbono respirado ao longo de seu transporte em direção às baixas latitudes do Atlântico Sul. Interessantemente, um registro de  $\delta^{13}\text{C}$  da termoclina no Sudoeste do Atlântico Sul não mostra grandes mudanças de  $\delta^{13}\text{C}$  durante os HS. Atribuímos essa diferença às distintas fontes de águas para a termoclina no Sudoeste Atlântico Sul, por um lado, e para a termoclina no Sudeste e Noroeste do Atlântico Sul, por outro. As águas da termoclina no Sudoeste do Atlântico Sul são provenientes da Água Modal Subtropical formada na Confluência Brasil-Malvinas, que sofre mistura com a Água Intermediária Antártica, diluindo o sinal de baixo  $\delta^{13}\text{C}$  do Oceano Austral que, de outra forma, é reconhecido no Sudeste e Noroeste do Atlântico Sul.

**Palavras-chave:** paleoceanografia, foraminíferos planctônicos da termoclina, isótopos estáveis de carbono, Atlântico Sul, Heinrich Stadials

## List of figures

**Figure 1.1.** Mean annual sea surface temperature (color shading) (Locarnini et al., 2018), schematic surface ocean circulation (black arrows) (Stramma and England, 1999) and atmospheric features (white arrows) of interest over the South Atlantic. Antarctic Circumpolar Current (ACC), Brazil Current (BC), Brazil–Malvinas Confluence (BMC), Intertropical Convergence Zone (ITCZ), Malvinas Current (MC), North Brazil Current (NBC), South Atlantic Current (SAC), Southern South Equatorial Current (SSEC), Subtropical Front (STF). The yellow stars depict the marine sediment cores investigated in this dissertation. 17

**Figure 2.1.** Location of marine sediment core M125-95-3 (yellow star) and other marine records discussed herein (open black dots). (a) Map of the modern relative abundance of planktonic foraminifera species *Globorotalia truncatulinoides* in the Atlantic Ocean<sup>23</sup>. Black dots represent the location of the surface sediment samples. The thin rectangle indicates the location of the temperature meridional profile depicted in panel “b”. (b) Mean annual temperature meridional profile for the upper 600 m of the water column of the Atlantic Ocean<sup>25</sup>. Vertical dotted lines delimit the South Atlantic Subtropical Gyre (SASG). See panel “a” for the location of the meridional profile. (c) Meridional profile of the modern relative abundance of *G. truncatulinoides* in the Atlantic Ocean<sup>23</sup>. The yellow star depicts the location of core M125-95-3 (this study) and the open black dot depicts the location of core MD07-3076Q<sup>24</sup>. (d) Mean annual sea surface temperature (color shading)<sup>25</sup>, schematic surface ocean circulation (black arrows)<sup>26</sup> and atmospheric features (white arrows) of interest over the South Atlantic. Antarctic Circumpolar Current (ACC), Brazil Current (BC), Brazil–Malvinas Confluence (BMC), Intertropical Convergence Zone (ITCZ), Malvinas Current (MC), North Brazil Current (NBC), South Atlantic Current (SAC), Southern South Equatorial Current (SSEC), Subtropical Front (STF). The location of the following cores are depicted: M35003-4<sup>27</sup>, GeoB3910-2<sup>28</sup>, M125-95-3 (this study), MD02-2594<sup>15</sup>, TN057-21<sup>14</sup>, MD07-3076Q<sup>24</sup>. This figure was produced using the Ocean Data View software<sup>29</sup> (ODV – version 5.2.1., <https://odv.awi.de>, 2020) and the CorelDRAW Graphics Suite software (CorelDRAW – version X6, <https://www.coreldraw.com>, 2012). 29

**Figure 2.2.** Comparison of relative abundance record of *Globorotalia truncatulinoides* from marine sediment core M125-95-3 with previously published records from the Atlantic Ocean. (a)  $^{231}\text{Pa}/^{230}\text{Th}$  from the Bermuda Rise<sup>35–37</sup>. (b) *Uvigerina* spp. stable carbon isotopic composition ( $\delta^{13}\text{C}$ ) from core M125-95-3 (running average of 3 points)<sup>38</sup>. (c) Relative abundance of *G. truncatulinoides* from core M125-95-3 (this study). (d)  $\text{In}(\text{Ti}/\text{Ca})$  from core GeoB3910-2 located in the northeastern Brazil<sup>28</sup>. Yellow stars on top of panel “c” depict calibrated radiocarbon ages and black triangles depict tie-points used to produce the age model of core M125-95-3 ( $2\sigma$  standard error smaller than symbol size)<sup>31</sup>. Blue vertical bars represent millennial-scale Heinrich Stadials (HS) 6-1 and the Younger Dryas (YD). Marine Isotope Stages (MIS) are depicted below the upper horizontal axis. Atlantic Meridional Overturning Circulation (AMOC), South Atlantic Subtropical Gyre (SASG), Intertropical Convergence Zone (ITCZ). 33

**Figure 2.3.** Relative abundance of *Globorotalia truncatulinoides* from cores M125-95-3 (this study) and MD07-3076Q<sup>24</sup> located at the northern and southern limits of the South Atlantic Subtropical Gyre (i.e., nSASG and sSASG), respectively together with other proxy records discussed herein. (a) Relative abundance of *G. truncatulinoides* from core M125-95-3 (this study). (b) Relative abundance of *G. truncatulinoides* from core MD07-3076Q (running average of 5 points) (note the inverted axis)<sup>24</sup>. (c) Mg/Ca-based sea surface temperatures in the Agulhas Leakage (running average of 3 points)<sup>15</sup>. (d) Ratio of the percentage of *Neogloboquadrina pachyderma* (sinistral; NPS) to total *N. pachyderma* (sinistral and dextral) from core TN057-21 (running average of 7 points)<sup>14</sup>. (e) Southern Ocean sea-ice presence (SIP) in the Atlantic and

Indian sectors of the Southern Ocean<sup>52,53</sup>. (f) Obliquity<sup>54</sup>. (g) Atmospheric CO<sub>2</sub> concentration<sup>55</sup>. Yellow stars on top of panel “b” depict calibrated radiocarbon ages and black triangles depict tie-points used to produce the age model of core M125-95-3 (2σ standard error smaller than symbol size)<sup>31</sup>. Blue vertical bars represent millennial-scale Heinrich Stadial (HS) 6 to 1 and the Younger Dryas (YD). Marine Isotope Stages (MIS) are depicted below the upper horizontal axis. Subtropical front (STF).

38

**Figure 2.4.** Schematic representation of the mechanism by which a southward displacement of the South Atlantic Subtropical Gyre during a Heinrich Stadial transfer more heat to the Southern Ocean, ultimately fostering CO<sub>2</sub> release to the atmosphere. This figure was produced using the Ocean Data View software<sup>29</sup> (ODV – version 5.2.1., <https://odv.awi.de>, 2020) and the CorelDRAW Graphics Suite software (CorelDRAW – version X6, <https://www.coreldraw.com>, 2012).

41

**Figure S5.1.** Relationship between the Atlantic Intertropical Convergence Zone and northern limit of the South Atlantic Subtropical Gyre (nSASG). (a) Bermuda Rise  $^{231}\text{Pa}/^{230}\text{Th}^{1-3}$ ; (b) δ<sup>13</sup>C *Uvigerina* spp. from the study site<sup>4</sup>; (c) Relative abundance of *Globorotalia truncatulinoides* from core M125-95-3; (d) %*Neogloboquadrina*/(%*Neogloboquadrina* + %*G. glutinata*) (RN/Gg) ratio as a proxy for the position of the Atlantic ITCZ in the Tobago Basin core M35003-4<sup>5</sup>; (e) Relative abundance of *Globorotalia truncatulinoides* from core M35003-4 (Tobago Basin)<sup>6</sup>. Yellow stars on top of panel “c” depict calibrated radiocarbon ages and black triangles depict tie-points used to produce the age model of core M125-95-3 (2σ standard error smaller than symbol size)<sup>2</sup>. Blue vertical bars represent millennial-scale Heinrich Stadials (HS) 6-1 and the Younger Dryas (YD). Marine Isotope Stages (MIS) are depicted below the upper horizontal axis. Atlantic Meridional Overturning Circulation (AMOC), Intertropical Convergence Zone (ITCZ), North Atlantic Subtropical Gyre (NASG), South Atlantic Subtropical Gyre (SASG).

49

## List of abbreviations

δ<sup>13</sup>C - Stable carbon isotopic composition

δ<sup>18</sup>O - Stable oxygen isotopic composition

δD - Stable deuterium isotopic composition

<sup>14</sup>C - Radiocarbon

AAIW - Antarctic Intermediate Water

AC - Agulhas Current (AC)

ACC - Antarctic Circumpolar Current (ACC)

AMOC - Atlantic Meridional Overturning Circulation

AMS - Accelerator Mass Spectrometry

BC - Brazil Current

BeC - Benguela Current

BMC - Brazil-Malvinas Confluence

CIME - Carbon Isotope Minimum Events

EDC - EPICA Dome C

HS - Heinrich Stadials

ITCZ - Intertropical Convergence Zone

MC - Malvinas Current

MIS - Marine Isotope Stages

NASG - North Atlantic Subtropical Gyre

NBC - North Brazil Current

SAC - South Atlantic Current

SACW - South Atlantic Central Water

SAMW - Subantarctic Mode Waters

SASG - South Atlantic Subtropical Gyre

SAZ - Subantarctic Zone

SEC - South Equatorial Current

SIP - Sea-Ice Presence

sNASG - southern boundary of the North Atlantic Subtropical Gyre

SO - Southern Ocean

sSASG - southern boundary of the South Atlantic Subtropical Gyre

SSEC - southern branch of the South Equatorial Current

SST – Sea surface temperature

STC - Subtropical Cells

STF - Subtropical Fronts

STMW - Subtropical Mode Waters

SWAF - South West Africa Campaign

TPG - Transitional to polar group

VPDB - Vienna Pee Dee Belemnite

YD - Younger Dryas

## Table of contents

<b><u>Resumo</u></b>	<b>ii</b>
<b><u>List of figures</u></b>	<b>iv</b>
<b><u>List of abbreviations</u></b>	<b>vi</b>
<b><u>Chapter 1</u></b>	<b>14</b>
<b><u>1.1 Introduction</u></b>	<b>14</b>
<b><u>1.2 Research objectives</u></b>	<b>17</b>
<b><u>1.3 Dissertation outline</u></b>	<b>18</b>
<b><u>1.4 References</u></b>	<b>20</b>
<b><u>Chapter 2</u></b>	<b>25</b>
<b><u>2. Meridional changes in the South Atlantic Subtropical Gyre during Heinrich Stadials</u></b>	<b>25</b>
<b><u>2.1 Introduction</u></b>	<b>26</b>
<b><u>2.2 Material and methods</u></b>	<b>30</b>
<b><u>2.2.1 Modern distribution of <i>Globorotalia truncatulinoides</i></u></b>	<b>30</b>
<b><u>2.2.2 Marine sediment core</u></b>	<b>31</b>
<b><u>2.2.3 Identification of planktonic foraminifera</u></b>	<b>31</b>
<b><u>2.2.4 Age model</u></b>	<b>32</b>
<b><u>2.3 Results</u></b>	<b>32</b>
<b><u>2.4 Discussion</u></b>	<b>34</b>
<b><u>2.4.1 Millennial-scale changes in the northern boundary of the South Atlantic Subtropical Gyre</u></b>	<b>34</b>
<b><u>2.4.2 Impacts of changes in the South Atlantic Subtropical Gyre</u></b>	<b>36</b>
<b><u>2.4.2.1 Southward migration of the South Atlantic Subtropical Gyre during Heinrich Stadials 6-4 and 1</u></b>	<b>38</b>
<b><u>2.4.2.2 Contraction of the South Atlantic Subtropical Gyre during Heinrich Stadials 3-2.....</u></b>	<b>39</b>
<b><u>2.5 Conclusions</u></b>	<b>42</b>
<b><u>2.6 References</u></b>	<b>42</b>
<b><u>Chapter 3</u></b>	<b>47</b>
<b><u>3. Millennial-scale negative <math>\delta^{13}\text{C}</math> excursions in the South Atlantic thermocline of the last glacial period</u></b>	<b>47</b>

<b><u>Chapter 4</u></b>	<b>47</b>
<b>4. <u>Concluding remarks and future challenges</u></b>	<b>47</b>
<b><u>Chapter 5</u></b>	<b>48</b>
<b>5. <u>Appendix 1 – Supplementary material to chapter 2</u></b>	<b>48</b>
<b>5.1 <u>Supplemantary references</u></b>	<b>50</b>

## Chapter 1

### 1.1 Introduction

Earth's is marked by a series of non-cyclic abrupt millennial-scale climate changes over the last glacial period. These episodes have been commonly associated to slowdown events in the strength of the Atlantic Meridional Overturning Circulation (AMOC) (i.e., Heinrich Stadials, (HS)) (Bohm et al., 2015; Henry et al., 2016; Lippold et al., 2016; McManus et al., 2004). The AMOC transfer a substantial amount of heat and salt to high latitudes in the North Atlantic (i.e., upper branch of the AMOC) (McCarthy et al., 2015; Trenberth and Caron, 2001). Once the upper branch of the AMOC reach high latitudes in the North Atlantic its heat content is released to the atmosphere (Lozier et al., 2019), and then, producing denser waters, which sinks at deep water formation sites and flows toward the South Atlantic (McCarthy et al., 2015; Rahmstorf, 2002). Therefore, slowdown events in the strength of the AMOC decrease/interrupt the heat transport towards the North Atlantic, resulting in intervals of heat accumulation in the Southern Hemisphere (Barker et al., 2009; Chiessi et al., 2015; Meier et al., 2021). Indeed, striking antiphase patterns between Greenland (cold events) and Antarctic (warm events) temperatures provide strong indications to the AMOC-related mechanism that has been widely validated by modelling results (e.g., Kageyama et al., 2013; Liu et al., 2009; Lohmann, 2003) as the main driver to the so-called *oceanic bipolar seesaw* (Crowley, 1992).

Independent lines of evidence point toward the southward shift of the Intertropical Convergence Zone (ITCZ) (Arz et al., 1999; Deplazes et al., 2013; Mulitz et al., 2017; Portilho-Ramos et al., 2017; Stríkis et al., 2015), forced by the weakened SST gradient, typically found during HS conditions (Chiang and Bitz, 2005). Synergistically, the Southern Hemisphere westerly winds also shift southward together with the ITCZ position (Anderson et al., 2009; Toggweiler and Lea, 2010). In response, the Southern Hemisphere Hadley Cell circulation and its subtropical jets strength are readjusted through atmospheric teleconnections by reducing them, which, in turn, allows strengthen Southern Hemisphere westerly winds (Denton et al., 2010). Such mechanism has forced changes in the Southern Ocean, for example, by enhancing the deep-water upwelling around the Antarctica (Anderson et al., 2009) and decreasing the iron fertilization, whereby the Southern Ocean's biological pump (Anderson et al., 2014; Martinez-Garcia et al., 2014). Both millennial-scale responses contribute to increases atmospheric CO<sub>2</sub> concentrations and therefore, are of fundamental importance to global climate variability.

Paleoceanographic studies provide evidences for latitudinal shifts of the Subtropical and the Subantarctic Fronts on orbital and millennial timescales (Bard and Rickaby, 2009; Barker et al., 2009; Barker and Diz, 2014; Dyez et al., 2014; Groeneveld and Chiessi, 2011; Peeters et al., 2004)). Under full glacial conditions (e.g., lowest seal level, largest sea ice expansion, and lowest atmospheric CO<sub>2</sub> concentration) large reductions in the exchange of heat and salt between the Indian and the Atlantic Oceans have been indicated, whereas the opposite response occurred during HS (Peeters et al., 2004; Chiessi et al., 2008). These contributions are quite valuable in order to constraint the past oceanic dynamics associated to the subtropical South Atlantic as well as its impact on the North Atlantic, for instance changes in the stability of the AMOC given by the enhancement of salt transport from the Indian Ocean (Ballalai et al., 2019).

In addition, another dominant ocean circulation feature responsible for redistributing energy between low and high latitudes are the subtropical gyres (Talley, 2003). In the South Atlantic, the South Atlantic Subtropical Gyre (SASG) behaves as a complementary mechanism related to the upper branch of the AMOC with a key role in the oceanic energy redistribution during HS (Pinho et al., 2021; Chapter 2). In fact, the SASG is characterized as a massive reservoir of heat and salt (Schmitz and McCartney, 1993). However, the past behavior and impact of the SASG remains unknown. In addition, paleoceanographic reconstructions of the subsurface (thermocline) circulation in the wide South Atlantic lacked either temporal resolution or spatial coverage to investigate abrupt millennial-scale climate changes (e.g., Chiessi et al., 2008; Campos et al., 2017; Santos et al., 2017, 2020; Venancio et al., 2018; Nascimento et al., 2021).

Comprehensive understanding of changes in the AMOC and its climate impacts back in time as a modern analogue is crucial since ongoing reductions in the strength of the AMOC have been already observed (e.g., Caesar et al., 2021, 2018; Rahmstorf et al., 2015; Thornalley et al., 2018) as well as the predicted ones until the end of this century regarding the greenhouse gases emission scenario (e.g., Weaver et al., 2012). Paleoceanographic records offer a great opportunity to identify long-term changes beyond the instrumental period for which increase the confidence level in climate model projections. Particularly, paleoceanographic findings support a close relationship between variations in the strength of the AMOC and drastic changes in Earth's climate and environments (Bouimetarhan et al., 2018; Campos et al., 2020; Chen et al., 2015; Crivellari et al., 2019; Höppner et al., 2018; Howe et al., 2018; Marcott et al., 2014; McManus et al., 2004; Venancio et al., 2020; Zular et al., 2019, 2020).

This Master's dissertation aims to contribute to fulfill the gap of knowledge on the paleoceanographic conditions of the upper South Atlantic during slowdown events in the strength of the AMOC over the last ca. 70 kyr. We investigate three marine sediment cores at key locations from the South Atlantic (i.e., NW-, SW- and SE-South Atlantic) (Fig. 1), by applying isotopic and micropaleontological proxies from planktonic foraminifera species at high-temporal resolution.

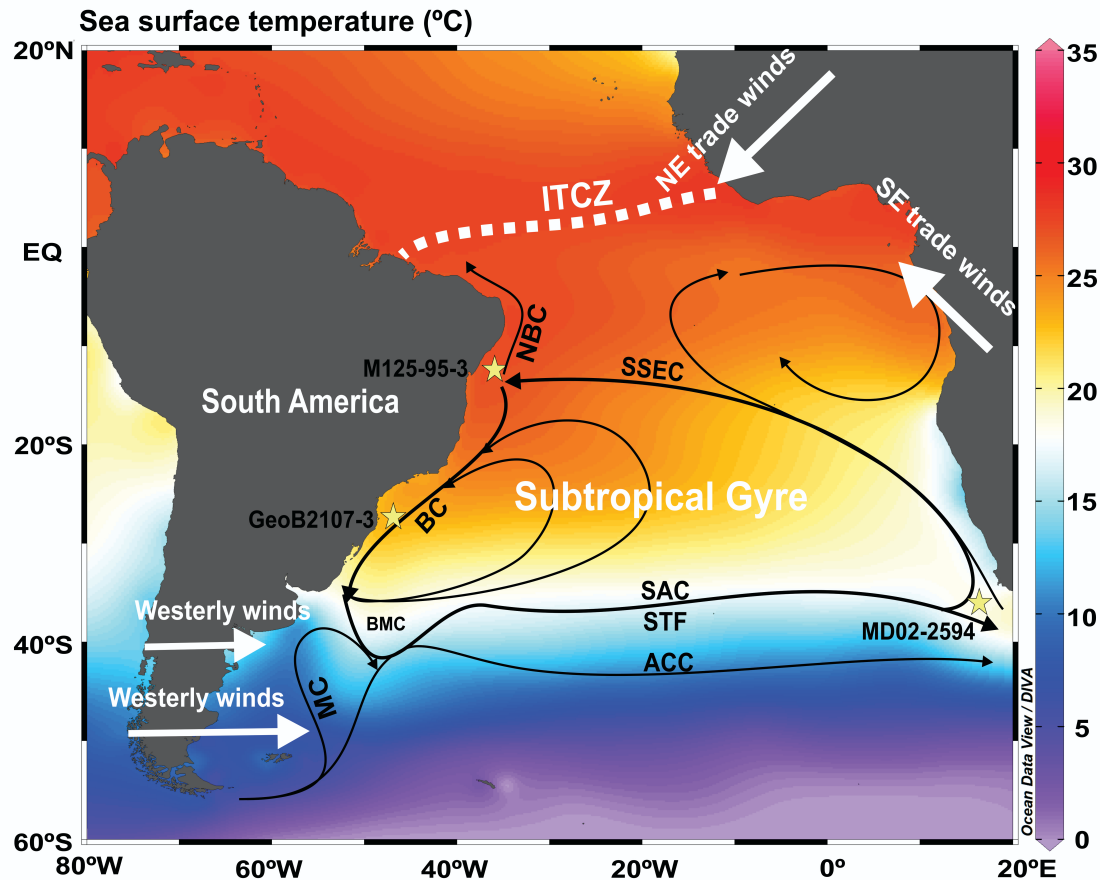


**Fig. 1.1.** Mean annual sea surface temperature (color shading) (Locarnini et al., 2018), schematic surface ocean circulation (black arrows) (Stramma and England, 1999) and atmospheric features (white arrows) of interest over the South Atlantic. Antarctic Circumpolar Current (ACC), Brazil Current (BC), Brazil–Malvinas Confluence (BMC), Intertropical Convergence Zone (ITCZ), Malvinas Current (MC), North Brazil Current (NBC), South Atlantic Current (SAC), Southern South Equatorial Current (SSEC), Subtropical Front (STF). The yellow stars depict the marine sediment cores investigated in this dissertation.

## 1.2 Research objectives

This Master's dissertation aims to reconstruct paleoceanographic changes of the upper South Atlantic from three marine sediment cores collected from the South Atlantic for the last glacial and deglacial abrupt millennial-scale climate changes stadials (i.e., HS). In order to reach this main aim, the following tasks were performed:

- Reconstruction of the upper water column stratification in the NW-South Atlantic related to changes in the northern limit of the South Atlantic Subtropical Gyre (nSASG) based on the relative abundance of the planktonic foraminifera species *Globorotalia truncatulinoides* from the core M125-95-3 ( $10.94^{\circ}\text{S}$ ,  $36.20^{\circ}\text{W}$ );
- Reconstruction of the variability in the South Atlantic Central Water (SACW) stable carbon isotopic composition ( $\delta^{13}\text{C}$ ) signature based on  $\delta^{13}\text{C}$  performed on thermocline-dwelling planktonic foraminifera species from three cores M125-95-3 ( $10.94^{\circ}\text{S}$ ,  $36.20^{\circ}\text{W}$ ; NW-South Atlantic), GeoB2107-3 ( $27.18^{\circ}\text{S}$ ,  $46.45^{\circ}\text{W}$ ; SW-South Atlantic; H.W. Arz, personal communication) and, MD02-2594

(34.71°S, 17.33°W; SE-South Atlantic; G. Martínez-Méndez, personal communication);

- Reconstruction of water mass contributions and changes in the circulation for the SACW based on thermocline-dwelling planktonic foraminifera species  $\delta^{13}\text{C}$  records from three cores M125-95-3, GeoB2107-3 (H.W. Arz, personal communication) and MD02-2594 (G. Martínez-Méndez, personal communication);
- Comparison of the data produced with records available in the literature.

### 1.3 Dissertation outline

In this Master's dissertation we present two manuscripts. In the first manuscript entitled "Meridional Changes in the South Atlantic Subtropical Gyre during Heinrich Stadials", recently published in Scientific Reports, (Chapter 2) we applied the relative abundance of *Globorotalia truncatulinoides* as a new proxy for the meridional displacement of the SASG. The modern distribution of its species along the Atlantic basin shows clearly a relationship with the SASG and NASG. Accordingly, we applied the percentage of *G. truncatulinoides* to our downcore record M125-95-3, which the core site is located in the nSASG. By comparing our record of its species with another one already published (Gottschalk et al., 2015) from a marine sediment core placed in the sSASG we identify an antiphase pattern during most of HS, indicating a southward migration of the SASG. However, it was not observed such pattern during HS3 and HS2, instead, in the sSASG the percentages remained unchanged, which suggest a meridional contraction. We propose that this dissimilarity was driven by full glacial boundary conditions reached by the period of the occurrence of HS3 and HS2 (i.e., at the end of Marine Isotope Stage (MIS) 3 and during most of MIS2). This comparative approach allows us to integrate the SASG as a whole regarding latitudinal shifts on millennial timescale. Importantly, we addressed the impact of changes in the SASG as a pivotal driver to the oceanic CO<sub>2</sub> outgassing in the Southern Ocean during millennial-scale stadials.

In the second manuscript entitled “Millennial-scale negative  $\delta^{13}\text{C}$  excursions in the South Atlantic thermocline of the last glacial period” (Chapter 3) we presented three thermocline-dwelling  $\delta^{13}\text{C}$  records at high temporal resolution from a set of marine sediment cores placed from the South Atlantic. The cores are located in the NW-South Atlantic (M125-95-3; 10.94°S, 36.20°W), SW-South Atlantic (GeoB2107-3; 27.18°S, 46.45°W; H.W. Arz, personal communication) and SE-South Atlantic (MD02-2594; 34.71°S, 17.33°W; G. Martínez-Méndez, personal communication). We have taken advantage of these core sites to investigate the thermocline circulation widely along the South Atlantic by analyzing thermocline-dwelling  $\delta^{13}\text{C}$  records. First, we went over the discussion on the potential of our  $\delta^{13}\text{C}$  records as water mass tracer. To achieve this goal we addressed and evaluated the multiple effects potentially affecting our  $\delta^{13}\text{C}$  records (e.g., local changes in nutrient content, air-sea gas exchange, carbonate ion concentration, symbiont activity, ontogenetic cycle, and further modifications by vital effects). All these analysis settle our  $\delta^{13}\text{C}$  records as a reliable water mass tracer, indeed.

The  $\delta^{13}\text{C}$  records between SE-South Atlantic and NW-South Atlantic thermoclines show an uncoupling long-term trend under full glacial boundary conditions during MIS3 / MIS2. We argue that this uncoupling trend could have been caused by a northward displacement of the Subtropical front under full glacial boundary conditions imposed in this time interval, whereby depleting locally the SE-South Atlantic thermocline  $\delta^{13}\text{C}$  signal. Our comparison between SE-South Atlantic and NW-South Atlantic thermocline  $\delta^{13}\text{C}$  records show negative excursions during most of HS. In addition, our NW-South Atlantic thermocline  $\delta^{13}\text{C}$  record displays higher negative  $\delta^{13}\text{C}$  excursions in comparison with the SE-South Atlantic. Instead, our SW-South Atlantic thermocline  $\delta^{13}\text{C}$  record shows no major and robust  $\delta^{13}\text{C}$  trends during HS. The negative excursions are driven by the strengthening of upwelling and an inefficient biological pump in the Southern Ocean. On top of that, we hypothesized the signal was further depleted by the aging effect, increasing the respired carbon accumulation along its transport until South Atlantic low latitudes, vis-à-vis our higher excursions in the NW-South Atlantic region. Contrastingly, we argue that the South Atlantic thermocline in our core site SW-South Atlantic could have been sourced by the Subtropical Mode Water formed at the Brazil-Malvinas Confluence by merging with Antarctic Intermediate Water, diluting the Southern Ocean low- $\delta^{13}\text{C}$  signal.

#### 1.4 References

Anderson, R.F., Ali, S., Bradtmiller, L.I., Nielsen, S.H.H., Fleisher, M.Q., Anderson, B.E.,

- Burckle, L.H., 2009. Wind-driven upwelling in the southern ocean and the deglacial rise in atmospheric CO<sub>2</sub>. *Science*. 323, 1443–1448. <https://doi.org/10.1126/science.1167441>
- Anderson, R.F., Barker, S., Fleisher, M., Gersonde, R., Goldstein, S.L., Kuhn, G., Mortyn, P.G., Pahnke, K., Sachs, J.P., 2014. Biological response to millennial variability of dust and nutrient supply in the Subantarctic South Atlantic Ocean. *Philos. Trans. R. Soc. A Math. Phys. Eng. Sci.* 372. <https://doi.org/10.1098/rsta.2013.0054>
- Arz, H.W., Pätzold, J., Wefer, G., 1999. The deglacial history of the western tropical Atlantic as inferred from high resolution stable isotope records off northeastern Brazil. *Earth Planet. Sci. Lett.* 167, 105–117. [https://doi.org/10.1016/S0012-821X\(99\)00025-4](https://doi.org/10.1016/S0012-821X(99)00025-4)
- Ballalai, J.M., Santos, T.P., Lessa, D.O., Venancio, I.M., Chiessi, C.M., Johnstone, H.J.H., Kuhnert, H., Claudio, M.R., Toledo, F., Costa, K.B., Albuquerque, A.L.S., 2019. Tracking Spread of the Agulhas Leakage Into the Western South Atlantic and Its Northward Transmission During the Last Interglacial. *Paleoceanogr. Paleoclimatology* 34, 1744–1760. <https://doi.org/10.1029/2019PA003653>
- Bard, E., Rickaby, R.E.M., 2009. Migration of the subtropical front as a modulator of glacial climate. *Nature* 460, 380–383. <https://doi.org/10.1038/nature08189>
- Barker, S., Diz, P., 2014. Timing of the descent into the last Ice Age determined by the bipolar seesaw. *Paleoceanography* 29, 489–507. <https://doi.org/10.1002/2014PA002623>
- Barker, S., Diz, P., Vautravers, M.J., Pike, J., Knorr, G., Hall, I.R., Broecker, W.S., 2009. Interhemispheric Atlantic seesaw response during the last deglaciation. *Nature* 457, 1097–1102. <https://doi.org/10.1038/nature07770>
- Bohm, E., Lippold, J., Gutjahr, M., Frank, M., Blaser, P., Antz, B., Fohlmeister, J., Frank, N., Andersen, M.B., Deininger, M., 2015. Strong and deep Atlantic meridional overturning circulation during the last glacial cycle. *Nature* 517, 73–76. <https://doi.org/10.1038/nature14059>
- Bouimetarhan, I., Chiessi, C.M., González-Arango, C., Dupont, L., Voigt, I., Prange, M., Zonneveld, K., 2018. Intermittent development of forest corridors in northeastern Brazil during the last deglaciation: Climatic and ecologic evidence. *Quat. Sci. Rev.* 192, 86–96. <https://doi.org/10.1016/j.quascirev.2018.05.026>
- Caesar, L., McCarthy, G.D., Thornalley, D.J.R., Cahill, N., Rahmstorf, S., 2021. Current Atlantic Meridional Overturning Circulation weakest in last millennium. *Nat. Geosci.* 14, 118–120. <https://doi.org/10.1038/s41561-021-00699-z>
- Caesar, L., Rahmstorf, S., Robinson, A., Feulner, G., Saba, V., 2018. Observed fingerprint of a weakening Atlantic Ocean overturning circulation. *Nature* 556, 191–196. <https://doi.org/10.1038/s41586-018-0006-5>
- Campos, M.C., Chiessi, C.M., Venancio, I.M., Pinho, T.M.L., Crivellari, S., Kuhnert, H., Schmiedl, G., Díaz, R.A., Albuquerque, A.L.S., Portilho-Ramos, R.C., Bahr, A., Multizzi, S., 2020. Constraining Millennial-Scale Changes in Northern Component Water Ventilation in the Western Tropical South Atlantic. *Paleoceanogr. Paleoclimatology* 35, 1–32. <https://doi.org/10.1029/2020PA003876>
- Campos, M.C., Chiessi, C.M., Voigt, I., Piola, A.R., Kuhnert, H., Multizzi, S., 2017. δ<sup>13</sup>C decreases in the upper western South Atlantic during Heinrich Stadials 3 and 2. *Clim. Past* 13, 345–358. <https://doi.org/10.5194/cp-13-345-2017>
- Chen, T., Robinson, L.F., Burke, A., Southon, J., Spooner, P., Morris, P.J., Ng, H.C., 2015. Synchronous centennial abrupt events in the ocean and atmosphere during the last deglaciation. *Science* (80-. ). 349, 1537–1541. <https://doi.org/10.1126/science.aac6159>
- Chiang, J.C.H., Bitz, C.M., 2005. Influence of high latitude ice cover on the marine Intertropical Convergence Zone. *Clim. Dyn.* 25, 477–496. <https://doi.org/10.1007/s00382-005-0040-5>

- Chiessi, C.M., Mulitza, S., Mollenhauer, G., Silva, J.B., Groeneveld, J., Prange, M., 2015. Thermal evolution of the western South Atlantic and the adjacent continent during Termination 1. *Clim. Past* 11, 915–929. <https://doi.org/10.5194/cp-11-915-2015>
- Chiessi, C.M., Mulitza, S., Paul, A., Pätzold, J., Groeneveld, J., Wefer, G., 2008. South Atlantic interocean exchange as the trigger for the Bølling warm event. *Geology* 36, 919. <https://doi.org/10.1130/G24979A.1>
- Crowley, T.J., 1992. North Atlantic Deep Water cools the southern hemisphere. *Paleoceanography* 7, 489–497. <https://doi.org/10.1029/92PA01058>
- Denton, G.H., Anderson, R.F., Toggweiler, J.R., Edwards, R.L., Schaefer, J.M., Putnam, A.E., 2010. The Last Glacial Termination. *Science* (80- ). 328, 1652–1656. <https://doi.org/10.1126/science.1184119>
- Deplazes, G., Lückge, A., Peterson, L.C., Timmermann, A., Hamann, Y., Hughen, K.A., Röhl, U., Laj, C., Cane, M.A., Sigman, D.M., Haug, G.H., 2013. Links between tropical rainfall and North Atlantic climate during the last glacial period. *Nat. Geosci.* 6, 213–217. <https://doi.org/10.1038/ngeo1712>
- Dyez, K.A., Zahn, R., Hall, I.R., 2014. Multicentennial Agulhas leakage variability and links to North Atlantic climate during the past 80,000-years. *Paleoceanography* 29, 1238–1248. <https://doi.org/10.1002/2014PA002698>
- Groeneveld, J., Chiessi, C.M., 2011. Mg/Ca of Globorotalia inflata as a recorder of permanent thermocline temperatures in the South Atlantic. *Paleoceanography* 26, 1–12. <https://doi.org/10.1029/2010PA001940>
- Henry, L.G., McManus, J.F., Curry, W.B., Roberts, N.L., Piotrowski, A.M., Keigwin, L.D., 2016. North Atlantic ocean circulation and abrupt climate change during the last glaciation. *Science* (80- ). 353, 470–474. <https://doi.org/10.1126/science.aaf5529>
- Höppner, N., Lucassen, F., Chiessi, C.M., Sawakuchi, A.O., Kasemann, S.A., 2018. Holocene provenance shift of suspended particulate matter in the Amazon River basin. *Quat. Sci. Rev.* 190, 66–80. <https://doi.org/10.1016/j.quascirev.2018.04.021>
- Howe, J.N.W., Huang, K.F., Oppo, D.W., Chiessi, C.M., Mulitza, S., Blusztajn, J., Piotrowski, A.M., 2018. Similar mid-depth Atlantic water mass provenance during the Last Glacial Maximum and Heinrich Stadial 1. *Earth Planet. Sci. Lett.* 490, 51–61. <https://doi.org/10.1016/j.epsl.2018.03.006>
- Kageyama, M., Merkel, U., Otto-Bliesner, B., Prange, M., Abe-Ouchi, A., Lohmann, G., Ohgaito, R., Roche, D.M., Singarayer, J., Swingedouw, D., 2013. Climatic impacts of fresh water hosing under Last Glacial Maximum conditions: a multi-model study. *Clim. Past* 9, 935–953. <https://doi.org/10.5194/cp-9-935-2013>
- Lippold, J., Gutjahr, M., Blaser, P., Christner, E., de Carvalho Ferreira, M.L., Mulitza, S., Christl, M., Wombacher, F., Böhm, E., Antz, B., Cartapanis, O., Vogel, H., Jaccard, S.L., 2016. Deep water provenance and dynamics of the (de)glacial Atlantic meridional overturning circulation. *Earth Planet. Sci. Lett.* 445, 68–78. <https://doi.org/10.1016/j.epsl.2016.04.013>
- Liu, Z., Otto-Bliesner, B.L., He, F., Brady, E.C., Tomas, R., Clark, P.U., Carlson, A.E., Lynch-Stieglitz, J., Curry, W., Brook, E., Erickson, D., Jacob, R., Kutzbach, J., Cheng, J., 2009. Transient Simulation of Last Deglaciation with a New Mechanism for Bølling-Allerød Warming. *Science* (80- ). 325, 310–314. <https://doi.org/10.1126/science.1171041>
- Locarnini, R.A., A.V. Mishonov, O.K. Baranova, T.P. Boyer, M.M. Zweng, H.E. Garcia, J.R. Reagan, D. Seidov, K.W. Weathers, C.R. Paver, and I.V.S. (2019)., 2019. World Ocean Atlas 2018 , Volume 1 : Temperature NOAA Atlas NESDIS 81 WORLD OCEAN ATLAS 2018 Volume 1 : Temperature National Oceanic and Atmospheric Administration. World Ocean Atlas 2018, Vol. 1 Temp. A. Mishonov, Tech. Ed. NOAA Atlas NESDIS 81,

- 52pp. 1, 52.
- Lohmann, G., 2003. Atmospheric and oceanic freshwater transport during weak Atlantic overturning circulation. *Tellus A Dyn. Meteorol. Oceanogr.* 55, 438–449. <https://doi.org/10.3402/tellusa.v55i5.12108>
- Lozier, M.S., Li, F., Bacon, S., Bahr, F., Bower, A.S., Cunningham, S.A., de Jong, M.F., de Steur, L., DeYoung, B., Fischer, J., Gary, S.F., Greenan, B.J.W., Holliday, N.P., Houk, A., Houpert, L., Inall, M.E., Johns, W.E., Johnson, H.L., Johnson, C., Karstensen, J., Koman, G., Le Bras, I.A., Lin, X., Mackay, N., Marshall, D.P., Mercier, H., Oltmanns, M., Pickart, R.S., Ramsey, A.L., Rayner, D., Straneo, F., Thierry, V., Torres, D.J., Williams, R.G., Wilson, C., Yang, J., Yashayaev, I., Zhao, J., 2019. A sea change in our view of overturning in the subpolar North Atlantic. *Science* (80-. ). 363, 516–521. <https://doi.org/10.1126/science.aau6592>
- Marcott, S.A., Bauska, T.K., Buzert, C., Steig, E.J., Rosen, J.L., Cuffey, K.M., Fudge, T.J., Severinghaus, J.P., Ahn, J., Kalk, M.L., McConnell, J.R., Sowers, T., Taylor, K.C., White, J.W.C., Brook, E.J., 2014. Centennial-scale changes in the global carbon cycle during the last deglaciation. *Nature* 514, 616–619. <https://doi.org/10.1038/nature13799>
- Martinez-Garcia, A., Sigman, D.M., Ren, H., Anderson, R.F., Straub, M., Hodell, D.A., Jaccard, S.L., Eglinton, T.I., Haug, G.H., 2014. Iron Fertilization of the Subantarctic Ocean During the Last Ice Age. *Science* (80-. ). 343, 1347–1350. <https://doi.org/10.1126/science.1246848>
- McManus, J.F., Francois, R., Gherard, J.M., Kelgwin, L., Drown-Leger, S., 2004. Collapse and rapid resumption of Atlantic meridional circulation linked to deglacial climate changes. *Nature* 428, 834–837. <https://doi.org/10.1038/nature02494>
- McCarthy, G.D., Smeed, D.A., Johns, W.E., Frajka-Williams, E., Moat, B.I., Rayner, D., Baringer, M.O., Meinen, C.S., Collins, J., Bryden, H.L., 2015. Measuring the Atlantic Meridional Overturning Circulation at 26°N. *Prog. Oceanogr.* 130, 91–111. <https://doi.org/10.1016/j.pocean.2014.10.006>
- Meier, K.J.F., Bahr, A., Chiessi, C.M., Albuquerque, A.L., Raddatz, J., Friedrich, O., 2021. Role of the Tropical Atlantic for the Interhemispheric Heat Transport During the Last Deglaciation. *Paleoceanogr. Paleoclimatology* 36. <https://doi.org/10.1029/2020PA004107>
- Mulitza, S., Chiessi, C.M., Schefuß, E., Lippold, J., Wichmann, D., Antz, B., Mackensen, A., Paul, A., Prange, M., Rehfeld, K., Werner, M., Bickert, T., Frank, N., Kuhnert, H., Lynch-Stieglitz, J., Portilho-Ramos, R.C., Sawakuchi, A.O., Schulz, M., Schwenk, T., Tiedemann, R., Vahlenkamp, M., Zhang, Y., 2017. Synchronous and proportional deglacial changes in Atlantic meridional overturning and northeast Brazilian precipitation. *Paleoceanography* 32, 622–633. <https://doi.org/10.1002/2017PA003084>
- Nascimento, R.A., Venancio, I.M., Chiessi, C.M., Ballalai, J.M., Kuhnert, H., Johnstone, H., Santos, T.P., Prange, M., Govin, A., Crivellari, S., Mulitza, S., Albuquerque, A.L.S., 2021. Tropical Atlantic stratification response to late Quaternary precessional forcing. *Earth Planet. Sci. Lett.* 568, 117030. <https://doi.org/10.1016/j.epsl.2021.117030>
- Peeters, F.J.C., Acheson, R., Brummer, G.J.A., De Ruijter, W.P.M., Schneider, R.R., Ganssen, G.M., Ufkes, E., Kroon, D., 2004. Vigorous exchange between the Indian and Atlantic oceans at the end of the past five glacial periods. *Nature* 430, 661–665. <https://doi.org/10.1038/nature02785>
- Pinho, T.M.L., Chiessi, C.M., Portilho-Ramos, R.C., Campos, M.C., Crivellari, S., Nascimento, R.A., Albuquerque, A.L.S., Bahr, A., Mulitza, S., 2021. Meridional changes in the South Atlantic Subtropical Gyre during Heinrich Stadials. *Sci. Rep.* 11, 9419. <https://doi.org/10.1038/s41598-021-88817-0>
- Portilho-Ramos, R.C., Chiessi, C.M., Zhang, Y., Mulitza, S., Kucera, M., Siccha, M., Prange,

- M., Paul, A., 2017. Coupling of equatorial Atlantic surface stratification to glacial shifts in the tropical rainbelt. *Sci. Rep.* 7. <https://doi.org/10.1038/s41598-017-01629-z>
- Rahmstorf, S., 2002. Ocean circulation and climate during the past 120,000 years. *Nature* 419, 207–214. <https://doi.org/10.1038/nature01090>
- Rahmstorf, S., Box, J.E., Feulner, G., Mann, M.E., Robinson, A., Rutherford, S., Schaffernicht, E.J., 2015. Exceptional twentieth-century slowdown in Atlantic Ocean overturning circulation. *Nat. Clim. Chang.* 5, 475–480. <https://doi.org/10.1038/nclimate2554>
- Santos, T.P., Lessa, D.O., Venancio, I.M., Chiessi, C.M., Mulitza, S., Kuhnert, H., Albuquerque, A.L.S., 2017. The Impact of the AMOC Resumption in the Western South Atlantic Thermocline at the Onset of the Last Interglacial. *Geophys. Res. Lett.* 44, 11,547–11,554. <https://doi.org/10.1002/2017GL074457>
- Schmitz, W.J., McCartney, M.S., 1993. On the North Atlantic Circulation. *Rev. Geophys.* 31, 29–49. <https://doi.org/10.1029/92RG02583>
- Stramma, L., England, M., 1999. On the water masses and mean circulation of the South Atlantic Ocean. *J. Geophys. Res. Ocean.* 104, 20863–20883. <https://doi.org/10.1029/1999JC900139>
- Stríkis, N.M., Chiessi, C.M., Cruz, F.W., Vuille, M., Cheng, H., de Souza Barreto, E.A., Mollenhauer, G., Kasten, S., Karmann, I., Edwards, R.L., Bernal, J.P., Sales, H. dos R., 2015. Timing and structure of Mega-SACZ events during Heinrich Stadial 1. *Geophys. Res. Lett.* 42, 5477–5484A. <https://doi.org/10.1002/2015GL064048>
- Talley, L.D., 2003. Shallow, intermediate, and deep overturning components of the global heat budget. *J. Phys. Oceanogr.* 33, 530–560. [https://doi.org/10.1175/1520-0485\(2003\)033<0530:SIADOC>2.0.CO;2](https://doi.org/10.1175/1520-0485(2003)033<0530:SIADOC>2.0.CO;2)
- Thornalley, D.J.R., Oppo, D.W., Ortega, P., Robson, J.I., Brierley, C.M., Davis, R., Hall, I.R., Moffa-Sánchez, P., Rose, N.L., Spooner, P.T., Yashayaev, I., Keigwin, L.D., 2018. Anomalously weak Labrador Sea convection and Atlantic overturning during the past 150 years. *Nature* 556, 227–230. <https://doi.org/10.1038/s41586-018-0007-4>
- Toggweiler, J.R., Lea, D.W., 2010. Temperature differences between the hemispheres and ice age climate variability. *Paleoceanography* 25. <https://doi.org/10.1029/2009PA001758>
- Trenberth, K.E., Caron, J.M., 2001. Estimates of Meridional Atmosphere and Ocean Heat Transports. *J. Clim.* 14, 3433–3443. [https://doi.org/10.1175/1520-0442\(2001\)014<3433:EOMAAO>2.0.CO;2](https://doi.org/10.1175/1520-0442(2001)014<3433:EOMAAO>2.0.CO;2)
- Venancio, I.M., Mulitza, S., Govin, A., Santos, T.P., Lessa, D.O., Albuquerque, A.L.S., Chiessi, C.M., Tiedemann, R., Vahlenkamp, M., Bickert, T., Schulz, M., 2018. Millennial- to Orbital-Scale Responses of Western Equatorial Atlantic Thermocline Depth to Changes in the Trade Wind System Since the Last Interglacial. *Paleoceanogr. Paleoclimatology* 33, 1490–1507. <https://doi.org/10.1029/2018PA003437>
- Venancio, I.M., Shimizu, M.H., Santos, T.P., Lessa, D.O., Portilho-Ramos, R.C., Chiessi, C.M., Crivellari, S., Mulitza, S., Kuhnert, H., Tiedemann, R., Vahlenkamp, M., Bickert, T., Sampaio, G., Albuquerque, A.L.S., Veiga, S., Nobre, P., Nobre, C., 2020. Changes in surface hydrography at the western tropical Atlantic during the Younger Dryas. *Glob. Planet. Change* 184, 103047. <https://doi.org/10.1016/j.gloplacha.2019.103047>
- Zular, A., Sawakuchi, A.O., Chiessi, C.M., D’Horta, F.M., Cruz, F.W., Demattê, J.A.M., Ribas, C.C., Hartmann, G.A., Giannini, P.C.F., Soares, E.A.A., 2019. The role of abrupt climate change in the formation of an open vegetation enclave in northern Amazonia during the late Quaternary. *Glob. Planet. Change* 172, 140–149. <https://doi.org/10.1016/j.gloplacha.2018.09.006>
- Zular, A., Sawakuchi, A.O., Wang, H., Guedes, C.C.F., Hartmann, G.A., Jaqueto, P.F., Chiessi,

- C.M., Cruz, F.W., Giannini, P.C.F., Daros, V.K., Atencio, D., Trindade, R.I.F., 2020. The response of a dune succession from Lençóis Maranhenses, NE Brazil, to climate changes between MIS 3 and MIS 2. *Quat. Int.* 537, 97–111. <https://doi.org/10.1016/j.quaint.2019.12.012>
- Weaver, A.J., Sedláček, J., Eby, M., Alexander, K., Crespin, E., Fichefet, T., Philippon Berthier, G., Joos, F., Kawamiya, M., Matsumoto, K., Steinacher, M., Tachiiri, K., Tokos, K., Yoshimori, M., Zickfeld, K., 2012. Stability of the Atlantic meridional overturning circulation: A model intercomparison. *Geophys. Res. Lett.* 39, 2012GL053763. <https://doi.org/10.1029/2012GL053763>

## Chapter 2

### 2. Meridional changes in the South Atlantic Subtropical Gyre during Heinrich Stadials

Tainá M. L. Pinho<sup>1\*</sup>; Cristiano M. Chiessi<sup>2</sup>; Rodrigo C. Portilho-Ramos<sup>3</sup>; Marília C. Campos<sup>1</sup>; Stefano Crivellari<sup>2</sup>; Rodrigo A. Nascimento<sup>4</sup>; Ana L.S. Albuquerque<sup>4</sup>; André Bahr<sup>5</sup>; Stefan Mulitza<sup>3</sup>

<sup>1</sup> Institute of Geosciences, University of São Paulo, São Paulo, Brazil

<sup>2</sup> School of Arts, Sciences and Humanities, University of São Paulo, São Paulo, Brazil

<sup>3</sup> MARUM – Center for Marine Environmental Sciences, University of Bremen,  
Bremen, Germany

<sup>4</sup> Graduate Program in Geochemistry, Fluminense Federal University, Niterói, Brazil

<sup>5</sup> Institute of Earth Sciences, Heidelberg University, Heidelberg, Germany

\* Correspondence and requests for materials should be addressed to T.M.L.P (email:

[taina.pinho@usp.br](mailto:taina.pinho@usp.br))

Published in **Scientific Reports (2021), 11, 9419**

<https://doi.org/10.1038/s41598-021-88817-0>

#### Abstract

Subtropical ocean gyres play a key role in modulating the global climate system redistributing energy between low and high latitudes. A poleward displacement of the subtropical gyres has been observed over the last decades, but the lack of long-term monitoring data hinders an in-depth understanding of their dynamics. Paleoceanographic records offer the opportunity to identify meridional changes in the subtropical gyres and investigate their consequences to the climate system. Here we use the abundance of planktonic foraminiferal species *Globorotalia truncatulinodes* from a sediment core collected at the northernmost boundary of the South Atlantic Subtropical Gyre (SASG) together with a

**previously published record of the same species from the southernmost boundary of the SASG to reconstruct meridional fluctuations of the SASG over last ca. 70 kyr. Our findings indicate southward displacements of the SASG during Heinrich Stadials (HS) 6-4 and HS1, and a contraction of the SASG during HS3 and HS2. During HS6-4 and HS1, the SASG southward displacements likely boosted the transfer of heat to the Southern Ocean, ultimately strengthening deep-water upwelling and CO<sub>2</sub> release to the atmosphere. We hypothesize that the ongoing SASG poleward displacement may further increase oceanic CO<sub>2</sub> release.**

## 2.1 Introduction

Subtropical gyres are large systems of anticyclonic upper ocean circulation driven by wind stress curl<sup>1,2</sup>, characterized as enormous reservoirs of heat and salt<sup>3</sup>. They are major pathways of energy redistribution between low and high latitudes with a pivotal role on the global climatic system<sup>4</sup>. As part of the subtropical gyres, western boundaries currents (e.g., Brazil Current (BC) and Gulf Stream) transport warm and salty tropical waters towards the poles, and eastern boundaries currents (e.g., Benguela and Canary Currents) transport cold and fresh waters towards the equator. At their midlatitude boundaries, subtropical gyres are limited by the Subtropical Fronts (STF).

Observational and model studies suggest a poleward migration of the subtropical gyres in the order of 0.1° per decade, driven by a systematic poleward displacement of the extratropical atmospheric circulation<sup>5</sup>. Changes in the geometry, strength and extension of the subtropical gyres may disturb the meridional heat transport with drastic consequences to marine ecosystems and the global climate system<sup>5,6</sup>. An increased heat content in most subtropical western boundary currents has been registered during the last decades (refs.<sup>7,8</sup>). In the western South Atlantic, warming of the BC has been claimed to cause a severe dwindling of commercial fish stocks<sup>9</sup>. Even total marine productivity is projected to decline due to the expansion of the “ocean deserts”, i.e., the oligotrophic subtropical gyres<sup>10,11</sup>. Yet, it is still not clear if modern changes in the subtropical gyres are promoted by anthropogenic activities or natural climate variability, mostly because of the relatively short instrumental observations. Paleoceanographic records offer a great opportunity to identify long-term changes in the subtropical gyres under different climatic conditions. This type of information is crucial to validate coupled climate models and improve our understanding of the potential anthropogenic role on the ongoing poleward shift of the subtropical gyres<sup>5</sup>.

Paleoceanographic studies provide evidences for latitudinal shifts of the Subtropical and the Subantarctic Fronts on orbital and millennial timescales (refs.<sup>12–16</sup>). In the Atlantic sector of the Southern Ocean, the northward displacement of the Subtropical and the Subantarctic Fronts during full glacials hampered the exchange of heat and salt between the Atlantic and the Indian oceans through the Agulhas Leakage<sup>12,16</sup>. In contrast, these fronts shifted southwards during millennial-scale climate events, e.g., Heinrich Stadials (HS)<sup>13,14</sup>. Despite the knowledge about the Subtropical and Subantarctic Fronts, the past behavior of the South Atlantic Subtropical Gyre (SASG) and its consequences for the climate system remain unknown.

*Globorotalia truncatulinoides* is a deep-dwelling planktonic foraminiferal species that calcifies its shells within the permanent thermocline<sup>17,18,19</sup>. This species presents an one-year reproductive cycle with extensive vertical migration in the water column that is highly dependent on the stratification of the upper ocean<sup>20,21</sup>. Therefore, *G. truncatulinoides* increases (decreases) in abundance when the thermocline is deeper

(shallower)<sup>19,21</sup>. The coiling direction of *G. truncatulinoides* has been commonly used to reconstruct the upper water column stratification<sup>21,22</sup>, although surface sediments from the Atlantic Ocean reveal that the distribution of both sinistral and dextral morphotypes of *G. truncatulinoides* are closely related to the subtropical gyres<sup>23</sup>, showing high abundance inside the gyres, where the thermocline is deeper, and being virtually absent to the north and south of the gyres, where the thermocline is shallower (Fig. 2.1a-c). Thus, the abundance of *G. truncatulinoides* in adequately located marine sediment cores is an excellent proxy to track meridional changes in the subtropical gyres.

Here we compare the relative abundance of *G. truncatulinoides* from two sediment cores located on opposite sides of the modern SASG (Fig. 2.1), which are key locations to track past meridional displacements of the SASG<sup>5</sup>. We provide a new record of *G. truncatulinoides* abundance from core M125-95-3 (10.94°S, 36.20°W, 1897m water depth) raised from the continental slope of the western tropical South Atlantic at the northern boundary of the SASG (nSASG) that covers the last ca. 70 kyr (Fig. 2.1a, d). We compare this record with the previously published abundance of *G. truncatulinoides* from core MD07-3076Q (44.92°S, 14.13°W, 3770m water depth)<sup>24</sup>, collected at the southern boundary of the SASG (sSASG) (Fig. 2.1a, d). High temporal-resolution data from both cores (ca. 518 and 223 yr, respectively, between adjacent samples) allow investigating millennial-scale changes in the SASG. The position of both cores has been strategically selected so that a meridional displacement of the SASG should cause antiphase excursions in *G. truncatulinoides* abundance in both cores. On the other hand, a contraction (expansion) of the SASG would cause a decrease (increase) in the abundance of *G. truncatulinoides* in both cores or a decrease (increase) in the abundance in one of the cores and no change in the other.

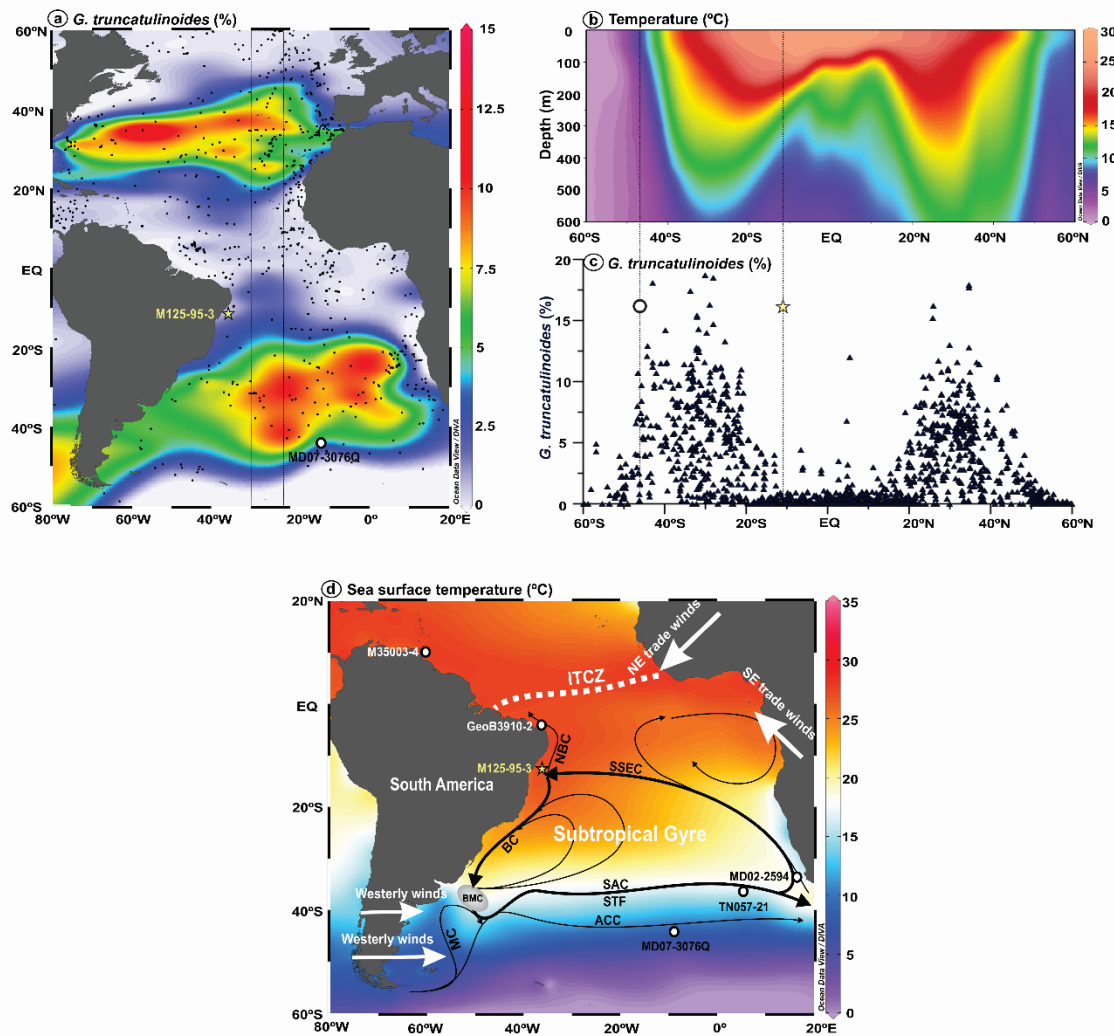


**Figure 2.1.** Location of marine sediment core M125-95-3 (yellow star) and other marine records discussed herein (open black dots). (a) Map of the modern relative abundance of planktonic foraminifera species *Globorotalia truncatulinoides* in the Atlantic Ocean<sup>23</sup>. Black dots represent the location of the surface sediment samples. The thin rectangle indicates the location of the temperature meridional profile depicted in panel “b”. (b) Mean annual temperature meridional profile for the upper 600 m of the water column of the Atlantic Ocean<sup>25</sup>. Vertical dotted lines delimit the South Atlantic Subtropical Gyre (SASG). See panel “a” for the location of the meridional profile. (c) Meridional profile of the modern relative abundance of *G. truncatulinoides* in the Atlantic Ocean<sup>23</sup>. The yellow star depicts the location of core M125-95-3 (this study) and the open black dot depicts the location of core MD07-3076Q<sup>24</sup>. (d) Mean annual sea surface temperature (color shading)<sup>25</sup>, schematic surface ocean circulation (black arrows)<sup>26</sup> and atmospheric features (white arrows) of interest over the South Atlantic. Antarctic Circumpolar Current (ACC), Brazil Current (BC), Brazil–Malvinas Confluence (BMC), Intertropical Convergence Zone (ITCZ), Malvinas Current (MC), North Brazil Current (NBC), South Atlantic Current (SAC), Southern South Equatorial Current (SSEC), Subtropical Front (STF). The location of the following cores are depicted: M35003-4<sup>27</sup>, GeoB3910-2<sup>28</sup>, M125-95-3 (this study), MD02-2594<sup>15</sup>, TN057-21<sup>14</sup>, MD07-3076Q<sup>24</sup>. This figure was produced using the Ocean Data View software<sup>29</sup> (ODV – version 5.2.1., <https://odv.awi.de>, 2020) and the CorelDRAW Graphics Suite software (CorelDRAW – version X6, <https://www.coreldraw.com>, 2012).

## 2.2 Material and methods

Piston core M125-95-3 was collected from the continental slope of the western tropical South Atlantic during RV Meteor cruise M125 (Fig. 2.1a, d)<sup>30</sup>. We focus on the uppermost 7.4 m of the core which spans the last ca. 70 kyr covering all HS of the last glacial and deglacial periods (the age model was previously published in ref.<sup>31</sup>). The age model is based on nine calibrated planktonic foraminifera accelerator mass spectrometry radiocarbon ages. For the portion of the core beyond the radiocarbon range, *Uvigerina* spp. stable oxygen isotopic ( $\delta^{18}\text{O}$ ) tie-points were tuned to a benthic  $\delta^{18}\text{O}$  reference curve from ref.<sup>32</sup>. The age modeling algorithm BACON v. 2.2<sup>33</sup> was used within the software PaleoDataView v. 0.8.3.4<sup>34</sup> to produce the age model. The relative abundance of planktonic foraminifera *G. truncatulinoides* were counted in the >150  $\mu\text{m}$  size fraction and its relative abundance was quantified from splits containing more than 300 specimens. We distinguished the sinistral and dextral morphotypes specimens of *G. truncatulinoides*, however, in the present study we choose to pool them together due to the very low abundance of the sinistral morphotype.

### 2.2.1 Modern distribution of *Globorotalia truncatulinoides*

The modern spatial distribution of planktonic foraminifera *Globorotalia truncatulinoides* in Atlantic Ocean sediments was extracted from Kucera *et al.*<sup>23</sup>. The comparison of its spatial distribution with upper water column structure, circulation and physico-chemical properties suggests that *G. truncatulinoides* track the meridional position of the South Atlantic Subtropical Gyre<sup>19,21,23</sup>. *Globorotalia truncatulinoides* shows high abundance inside the gyre where the thermocline is deep, and is virtually absent to the north and south of the gyre where the thermocline is shallow. In Kucera *et al.*<sup>23</sup>, foraminifera were picked from the >150  $\mu\text{m}$  size fraction of sample splits containing around 300 specimens<sup>23</sup>, the same method applied here. Further details on the ages of modern surface sediments can be found in Kucera *et al.*<sup>23</sup>. Modern foraminiferal data used here are available from the World Data Center PANGAEA (<https://doi.pangaea.de/10.1594/PANGAEA.841194>).

### 2.2.2 Marine sediment core

Marine sediment core M125-95-3 (10.94°S, 36.20°W, 1897m water depth, 1040 cm long) was collected from the continental slope of the western tropical South Atlantic during RV Meteor cruise M125<sup>30</sup>. Here we examined the upper 740 cm of the core that span the last ca. 70 kyr and cover all Heinrich Stadials (HS) of the last glacial and deglacial periods. This section was sampled with 10  $\text{cm}^3$  syringes. Samples were wet-sieved, oven-dried at 50°C and the size fraction higher than 125  $\mu\text{m}$  was stored in glass vials. Faunal analyses were conducted every 10 cm for the whole investigated section but sampling space was decreased in the neighborhood and within every HS. 144 samples were analyzed.

### 2.2.3 Identification of planktonic foraminifera

The wet-sieved and oven-dried > 125  $\mu\text{m}$  fraction was dry-sieved in a 150  $\mu\text{m}$  sieve, and the > 150  $\mu\text{m}$  fraction was used for the determination of the relative abundances of the species that were quantified from splits containing more than 300 specimens. Taxonomy was based on Stainforth *et al.*<sup>68</sup> and Hemleben *et al.*<sup>69</sup>). Here we present the abundance of planktonic foraminifera species *Globorotalia truncatulinoides* (both dextral and sinistral morphotypes). Since sediment core M125-95-3 was collected well above the glacial lysocline depth<sup>70</sup>, we considered the effect of dissolution in our planktonic foraminiferal faunal composition to be negligible. The planktonic

foraminifera *G. truncatulinoides* record from sediment core MD07-3076Q was previously published by *Gottschalk et al.*<sup>24</sup>.

#### 2.2.4 Age model

The age model of sediment core M125-95-3 was previously published by *Campos et al.*<sup>31</sup>. It combines nine calibrated planktonic foraminifera accelerator mass spectrometry radiocarbon ages and tuning benthic foraminifera  $\delta^{18}\text{O}$  tie-points to a benthic  $\delta^{18}\text{O}$  reference curve from *Govin et al.*<sup>32</sup>. The age modeling algorithm BACON v. 2.2<sup>33</sup> was used within the software PaleoDataView v. 0.8.3.4<sup>34</sup> for age-depth modeling.

### 2.3 Results

The relative abundance of *G. truncatulinoides* in core M125-95-3 ranges between 0 and 5.9 %, with mean value of 1.7 % during the last glacial period and 0.8 % during the Holocene (Fig. 2.2c). Millennial-scale negative excursions of up to 5.9 % characterize the relative abundance record of *G. truncatulinoides* and coincide with all HS of the last glacial and deglacial periods.

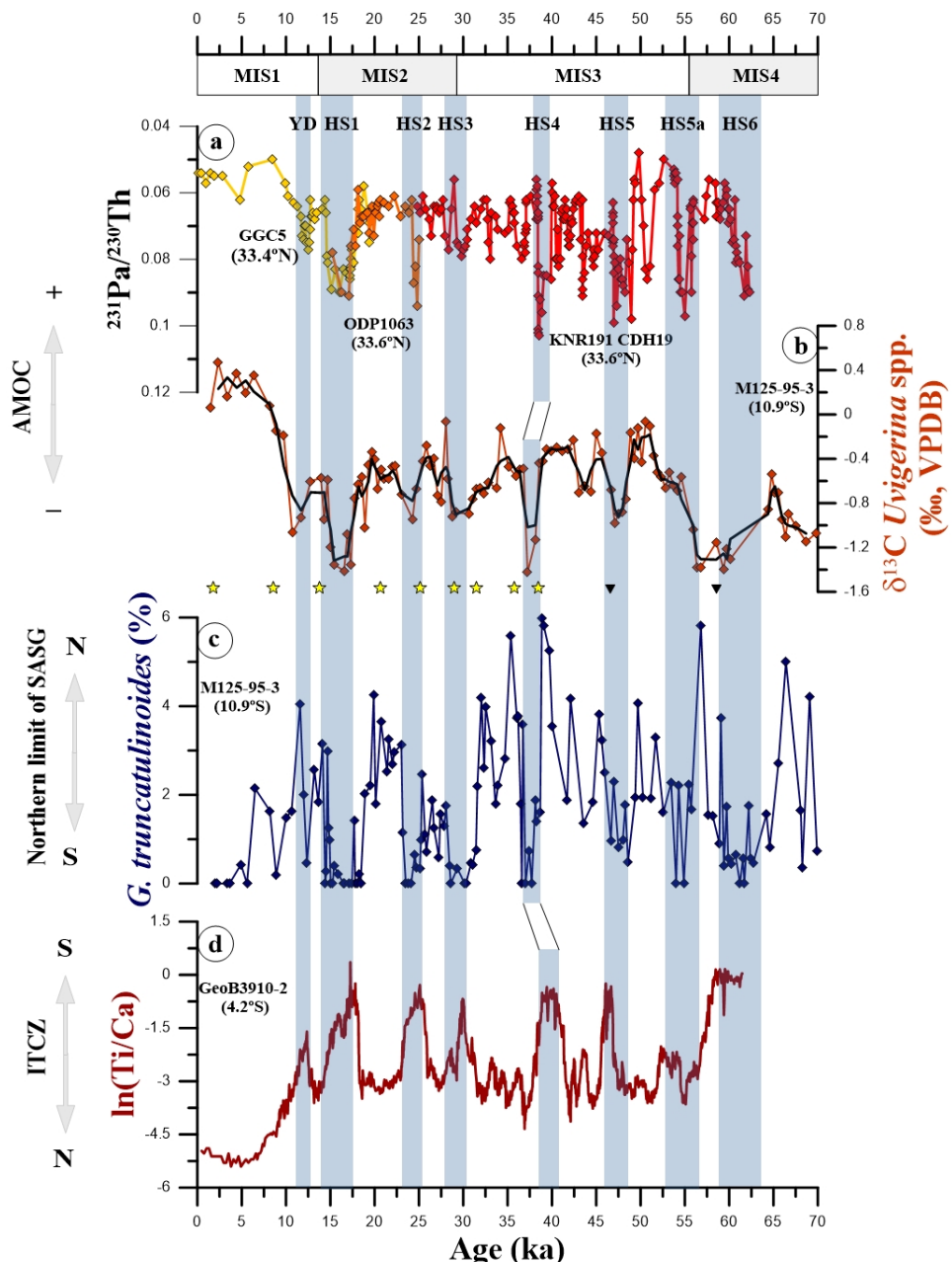


**Figure 2.2.** Comparison of relative abundance record of *Globorotalia truncatulinoides* from marine sediment core M125-95-3 with previously published records from the Atlantic Ocean. (a)  $^{231}\text{Pa}/^{230}\text{Th}$  from the Bermuda Rise<sup>35–37</sup>. (b) *Uvigerina* spp. stable carbon isotopic composition ( $\delta^{13}\text{C}$ ) from core M125-95-3 (running average of 3 points)<sup>38</sup>. (c) Relative abundance of *G. truncatulinoides* from core M125-95-3 (this study). (d)  $\ln(\text{Ti/Ca})$  from core GeoB3910-2 located in the northeastern Brazil<sup>28</sup>. Yellow stars on top of panel “c” depict calibrated radiocarbon ages and black triangles depict tie-points used to produce the age model of core M125-95-3 ( $2\sigma$  standard error smaller than symbol size)<sup>31</sup>. Blue vertical bars represent millennial-scale Heinrich Stadials (HS) 6-1 and the Younger Dryas (YD). Marine Isotope Stages (MIS) are depicted below the upper horizontal axis. Atlantic Meridional Overturning Circulation (AMOC), South Atlantic Subtropical Gyre (SASG), Intertropical Convergence Zone (ITCZ).

## 2.4 Discussion

#### 2.4.1 Millennial-scale changes in the northern boundary of the South Atlantic Subtropical Gyre

The decreases in the relative abundance of *G. truncatulinoides* occurred simultaneously with increases in precipitation over NE Brazil that were, in turn, associated to southward displacements in the Intertropical Convergence Zone (ITCZ) during HS (Fig. 2.2c-d)<sup>28,39</sup>. The meridional position of the ITCZ determines the location of the equatorial ascending branch of the Hadley Cells. The Hadley Cells from both hemispheres have an important role in the interhemispheric atmospheric heat transport<sup>40</sup>. Under a weak Atlantic Meridional Overturning Circulation (AMOC) (e.g., during HS) (Fig. 2.2a-b)<sup>35–37</sup>, the decreased northward oceanic heat transport warmed the South Atlantic<sup>13,41</sup>. This resulted in a southward migration of the equatorial ascending branch of the Hadley Cells, partially compensating the decrease in northward oceanic heat transport via an increase in the northward atmospheric heat transport<sup>42,43</sup>.

Changes in the Hadley Cells directly affect the oceanic Subtropical Cells (STC) by changing the trade winds stress on the surface. Indeed, the wind-driven oceanic STC can be described as the upper ocean counter-part of the Hadley Cells<sup>44</sup>. Therefore, changes in the meridional position of the equatorial branch of the STC are linked to the ITCZ position via the Hadley Cells<sup>45</sup>. During HS, McGee *et al.*<sup>43</sup> described a southward shift of the ascending branch of the South Atlantic STC that followed the ITCZ<sup>43</sup>. The southward shift of the STC in the South Atlantic should be accompanied by a southward displacement of the nSASG during HS. We suggest that southward migrations of the nSASG during HS increased the upper water column stratification (i.e., shallower thermocline) at our core site (10.94°S, 36.20°W), decreasing the abundance of *G. truncatulinoides* (Figs. 2.2c, 2.3a). An increased stratification in the upper water column of the western tropical South Atlantic during HS has been confirmed by Portilho-Ramos *et al.*<sup>46</sup> and Pedro *et al.*<sup>47</sup> (Fig. S5.1d), supporting our suggestion.

In line with our results, in the tropical North Atlantic at the southern boundary of the North Atlantic Subtropical Gyre (sNASG), increases in the abundance of *G. truncatulinoides* (Fig. S5.1e)<sup>27</sup> during HS suggest southward migrations of the sNASG. This is supported by upper water column temperature and salinity data<sup>48</sup>, as well as model experiments<sup>49</sup>, suggesting a tight coupling between the ascending branches of both STC and subtropical gyres in the Atlantic during HS.

The suggested southward migrations of the nSASG during HS were also accompanied by decreases in the strength of the SE trade winds<sup>50</sup>, that, in turn, are a consequence of the decreased meridional sea-surface temperature (SST) gradient in the tropical South Atlantic<sup>13</sup>. The reduced strength of the SE trade winds was thus co-responsible for the increases in upper water column stratification in the western tropical South Atlantic. At our core site, however, the large amplitude decreases in the abundance of *G. truncatulinoides* (Figs. 2.2c, 2.3a) point to the occurrence of changes in upper water column structure. Such changes would be accomplished by the nSASG crossing southwards our core site (Fig. 2.1).

Moreover, our core site is located at the modern bifurcation of the South Equatorial Current (SEC) in the upper 100 m of the water column (Fig. 2.1d). Our suggestion of southward migrations of the nSASG to be dynamically linked to southward shifts of the ITCZ position during HS contrasts to the seasonal mode of changes in the SEC bifurcation (i.e., during austral summer, a southward migration of the ITCZ occurs simultaneously to a northward migration of the SEC bifurcation)<sup>51</sup>. Thus, our results highlight the need to consider the timescale while investigating the processes

responsible for changes in western tropical South Atlantic upper water column stratification.

#### 2.4.2 Impacts of changes in the South Atlantic Subtropical Gyre

The *G. truncatulinoides* abundance records from the nSASG (core M125-95-3) and the sSASG (core MD07-3076Q) reveal an antiphase pattern during HS6-4 and HS1 (Fig. 2.3a–b). Notably, in both *G. truncatulinoides* records sinistral and dextral morphotypes were quantified together. While in the nSASG *G. truncatulinoides* abundance decrease during HS6-1 (Fig. 2.3a), in the sSASG *G. truncatulinoides* abundance increase during HS6-4 and HS1 with no clear trend during HS3 and HS2 (Fig. 2.3b)<sup>24</sup>. The antiphase pattern suggests that the whole SASG was displaced southwards during HS6-4 and HS1. In contrast, the reduction in *G. truncatulinoides* in the nSASG together with constant values in the sSASG suggest a meridional contraction of the SASG during HS3 and HS2 (Fig. 2.3a–b).

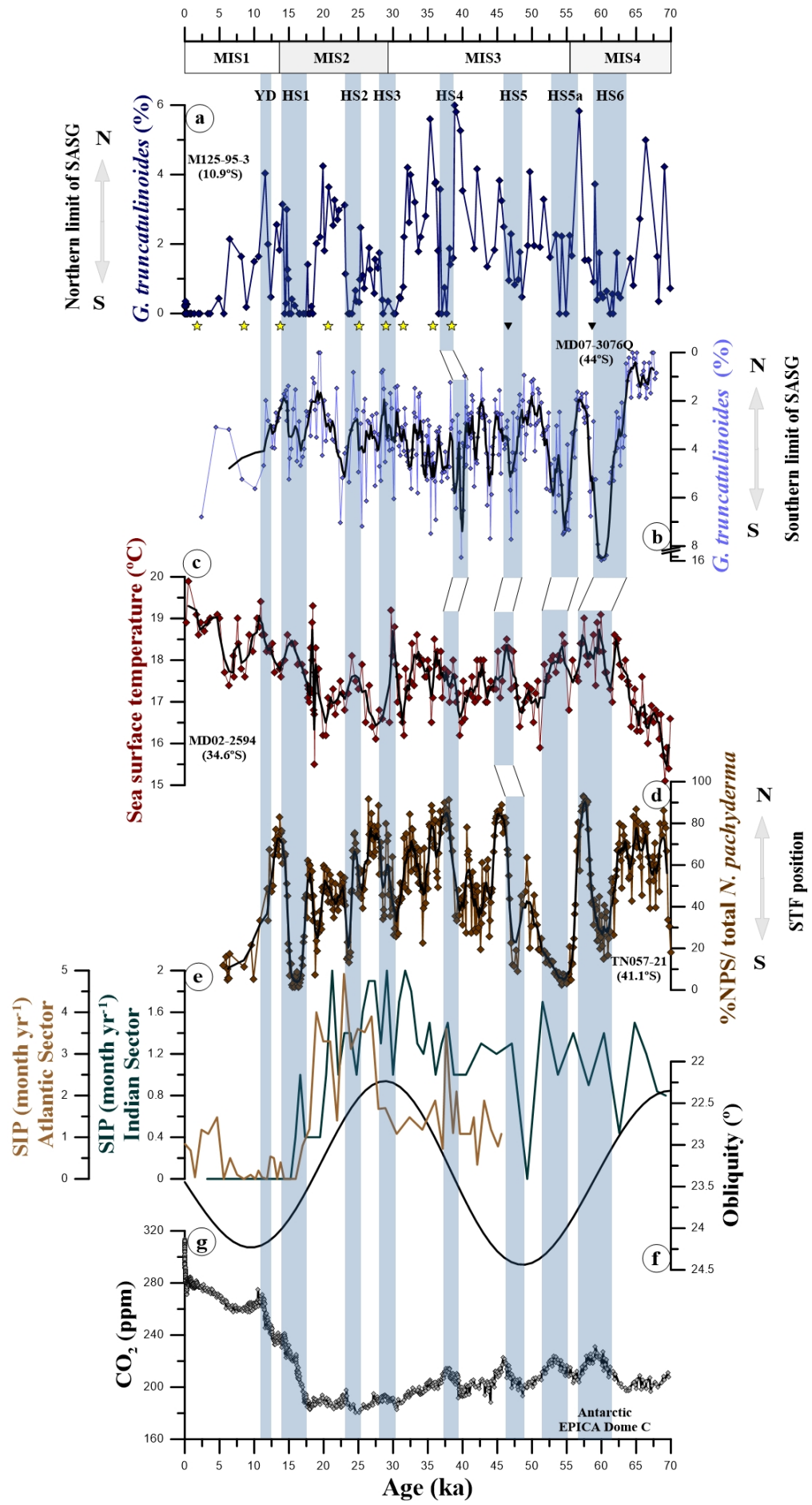


**Figure 2.3.** Relative abundance of *Globorotalia truncatulinoides* from cores M125-95-3 (this study) and MD07-3076Q<sup>24</sup> located at the northern and southern limits of the South Atlantic Subtropical Gyre (i.e., nSASG and sSASG), respectively together with other proxy records discussed herein. (a) Relative abundance of *G. truncatulinoides* from core M125-95-3 (this study). (b) Relative abundance of *G. truncatulinoides* from core MD07-3076Q (running average of 5 points) (note the inverted axis)<sup>24</sup>. (c) Mg/Ca-based sea surface temperatures in the Agulhas Leakage (running average of 3 points)<sup>15</sup>. (d) Ratio of the percentage of *Neogloboquadrina pachyderma* (sinistral; NPS) to total *N. pachyderma* (sinistral and dextral) from core TN057-21 (running average of 7 points)<sup>14</sup>. (e) Southern Ocean sea-ice presence (SIP) in the Atlantic and Indian sectors of the Southern Ocean<sup>52,53</sup>. (f) Obliquity<sup>54</sup>. (g) Atmospheric CO<sub>2</sub> concentration<sup>55</sup>. Yellow stars on top of panel “b” depict calibrated radiocarbon ages and black triangles depict tie-points used to produce the age model of core M125-95-3 (2σ standard error smaller than symbol size)<sup>31</sup>. Blue vertical bars represent millennial-scale Heinrich Stadial (HS) 6 to 1 and the Younger Dryas (YD). Marine Isotope Stages (MIS) are depicted below the upper horizontal axis. Subtropical front (STF).

#### 2.4.2.1 Southward migration of the South Atlantic Subtropical Gyre during Heinrich Stadials 6-4 and 1

The Southern Hemisphere westerly winds control the position of the STF in the South Atlantic (e.g., ref.<sup>56</sup>). A southward displacement of the STF during HS has been suggested<sup>57</sup>. The concurrent HS increases in the abundance of *G. truncatulinoides* in the sSASG (Fig. 2.3b) and the decreases in dust flux around Antarctica (a proxy for the Southern Hemisphere westerly winds intensity) suggest a link between the southward displacements of the sSASG and the Southern Hemisphere westerly winds<sup>58</sup>. The southward (northward) displacement of the STF has commonly been correlated to the increased (reduced) water inflow from the Indian to the Atlantic Ocean through the Agulhas Leakage<sup>59,60</sup>. A SST record under the influence of the Agulhas Leakage indeed shows systematic millennial-scale increases during HS, indicating southward shifts of the STF (Fig. 2.3c)<sup>15</sup>. Also, a planktonic foraminiferal index for the relative position of the STF in the South Atlantic (% *Neogloboquadrina pachyderma* (sinistral) / *N. pachyderma* total) corroborates the southward migrations of the STF during HS (Fig. 2.3d)<sup>14</sup>. The strong correlation between the *G. truncatulinoides* record from the sSASG, Agulhas Leakage SST and the STF index (Fig. 2.3b-d) suggest that the position of the sSASG was closely related to the Southern Hemisphere westerly winds and the STF. We suggest that the extratropical atmospheric circulation accompanied the southward displacement of the ITCZ and the nSASG during the HS6-4 and HS1, as indicated by model experiments<sup>43</sup>.

Model simulations of a collapsed AMOC show a positive temperature anomaly (ca. 4°C) at ca. 500 m water depth in the SASG and a deepening in the thermocline in the sSASG<sup>47</sup>, indications of an increase in the heat content of the SASG and a southward shift in the sSASG, respectively. Concurrently, in the Antarctic Circumpolar Current the increased eddy heat transport together with a southern position of the westerlies, likely allowed for more heat to reach high southern latitudes causing a retreat in Antarctic sea ice<sup>47,61</sup>. The southward displacement of the sSASG probably produced a steeper meridional SST gradient in the mid-latitudes of the South Atlantic. This steeper gradient may have contributed to stronger and southward-shifted westerlies, strengthening Southern Ocean deep-water upwelling<sup>62</sup>. Increased upwelling around Antarctica, in turn, fostered CO<sub>2</sub> release to the atmosphere<sup>63</sup>. A weakened dust-driven biological pump in

the Southern Ocean also contributed to the rise in atmospheric CO<sub>2</sub> during HS (e.g., ref.<sup>64</sup>) (Fig. 2.3g).

#### 2.4.2.2 *Contraction of the South Atlantic Subtropical Gyre during Heinrich Stadials 3-2*

Decreases in *G. truncatulinoides* abundance at the nSASG and the absence of major changes in the abundance of this species at the sSASG (Fig. 2.3a–b) suggest a meridional contraction of the SASG during HS3 and HS2. At the end of Marine Isotope Stage (MIS) 3 and during most of MIS2, the abundance of *G. truncatulinoides* at the sSASG<sup>24</sup> shows nearly constant values between 2-4% (Fig. 2.3b). This is the period (i.e., ca. 30-19 ka) when full glacial boundary conditions (e.g., lowest seal level, largest sea ice expansion, and lowest atmospheric CO<sub>2</sub> concentration) were reached. This period encompasses HS3 and HS2, which were not related to southward shifts of the sSASG (Fig. 2.3b). We suggest that the full glacial boundary conditions hindered the sSASG to migrate southwards even under HS forcing. Under full glacial boundary conditions, the northward migration of the Polar and Subantarctic Fronts together with extensive sea-ice around Antarctica probably hampered southward displacements of the sSASG. The striking increase in sea-ice in the Atlantic and Indian sectors of the Southern Ocean under full glacial boundary conditions corroborates this suggestion (Fig. 2.3e)<sup>52,53</sup>. The long-term expansion of sea-ice equatorwards was fostered by low obliquity<sup>65</sup> that reached minimum value at ca. 30 ka (Fig. 2.3f)<sup>54</sup>. Changes in sea-ice extent should be accompanied by changes in the oceanic Polar and Subantarctic Fronts (e.g., refs.<sup>12,16,66,67</sup>). Records on millennial-scale temporal resolution of the Agulhas Leakage SST, the position of the STF and dust flux to the Southern Ocean (Fig. 2.3c–d)<sup>14,15,58</sup> confirm the presence of full glacial boundary conditions during HS3 and HS2. Importantly, full glacial boundary conditions were associated to a significant northward displacement of the Southern Hemisphere westerly winds and a marked decrease in Southern Ocean deep-water upwelling, that hindered CO<sub>2</sub> to be released from the Southern Ocean to the atmosphere, as recorded in ice-cores during HS3 and HS2 (Fig. 2.3e–g)<sup>55</sup>.

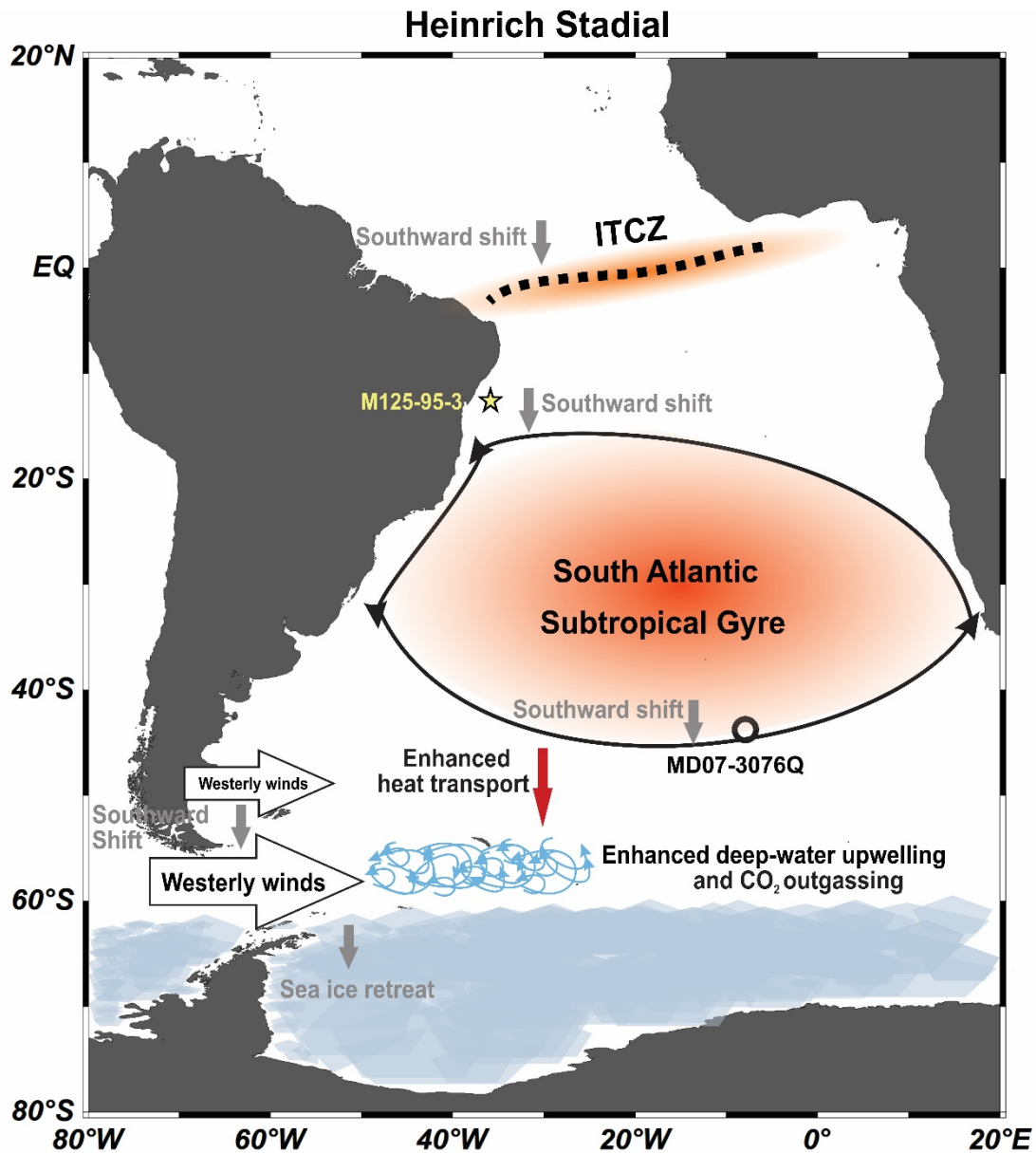


**Figure 2.4.** Schematic representation of the mechanism by which a southward displacement of the South Atlantic Subtropical Gyre during a Heinrich Stadial transfer more heat to the Southern Ocean, ultimately fostering CO<sub>2</sub> release to the atmosphere. This figure was produced using the Ocean Data View software<sup>29</sup> (ODV – version 5.2.1., <https://odv.awi.de>, 2020) and the CorelDRAW Graphics Suite software (CorelDRAW – version X6, <https://www.coreldraw.com>, 2012).

In summary, enhanced poleward heat fluxes occurred during HS6-4 and HS1 and were favored by southward shifts of the SASG (Fig. 2.4). Such meridional migrations of the SASG may have played a central role on oceanic carbon storage or release during the last glacial period on millennial timescales by controlling heat delivery to the Southern Ocean (Fig. 2.4). Regarding the ongoing poleward displacement of the SASG<sup>5</sup>, our results suggest that an increase in heat transport to the Southern Ocean may strengthen deep-water upwelling and CO<sub>2</sub> release to the atmosphere, constituting a positive feedback for global warming.

## 2.5 Conclusions

Here we present the abundance of *G. truncatulinoides* as a new proxy for the meridional displacement of the SASG on millennial timescales. Our *G. truncatulinoides* abundance record, together with previously published records, show that the SASG migrated southwards during most HS of the last glacial and deglacial periods (i.e., HS6-4 and HS1). These events were probably responsible for the transfer of substantial amounts of heat from the SASG to the Southern Ocean, ultimately strengthening deep-water upwelling and CO<sub>2</sub> release to the atmosphere. On the other hand, the SASG contracted during HS3 and HS2, likely resulting in decreased poleward heat transfer, deep-water upwelling and CO<sub>2</sub> release to the atmosphere. The contraction was forced by full glacial boundary conditions, namely equatorwards advance in sea-ice as well as in the position of the Polar and Subantarctic Fronts. While several studies previously described the release of CO<sub>2</sub> to the atmosphere during millennial-scale stadials, our novel mechanism suggests that the poleward heat transfer from the SASG to the Southern Ocean had a pivotal role in this process. Our results indicate that the ongoing poleward displacement of the SASG may drive oceanic CO<sub>2</sub> release that will act as a positive feedback to global warming.

## 2.6 References

1. Rui Xin Huang, & Russell, S. Ventilation of the subtropical north Pacific. *J. Phys. Oceanogr.* **24**, 2589–2605 (1994).
2. Munk, W. H. On the wind-driven ocean circulation. *J. Meteorol.* **7**, 80–93 (1950).
3. Schmitz, W. J., & McCartney, M. S. On the North Atlantic Circulation. *Rev. Geophys.* (1993).
4. Talley, L. D. Shallow, intermediate, and deep overturning components of the global heat budget. *J. Phys. Oceanogr.* **33**, 530–560 (2003).
5. Yang, H. *et al.* Poleward Shift of the Major Ocean Gyres Detected in a Warming Climate. *Geophys. Res. Lett.* **47**, (2020).
6. Marcello, F. & Wainer, I. South Atlantic Subtropical Gyre Late Twentieth Century Changes. *J. Geophys. Res. Ocean.* **123**, 5194–5209 (2018).
7. Wu, L. *et al.* Enhanced warming over the global subtropical western boundary currents. *Nat. Clim. Chang.* **2**, 161–166 (2012).
8. Yang, H. *et al.* Intensification and poleward shift of subtropical western boundary currents in a warming climate. *J. Geophys. Res. Ocean.* **121**, 4928–4945 (2016).
9. Auad, G. & Martos, P. Climate Variability of the Northern Argentinean Shelf Circulation: Impact on Engraulis Anchoita. *Int. J. Ocean Clim. Syst.* **3**, 17–43 (2012).
10. Polovina, J. J., Howell, E. A. & Abecassis, M. Ocean’s least productive waters are expanding. *Geophys. Res. Lett.* **35**, 2–6 (2008).
11. Irwin, A. J. & Oliver, M. J. Are ocean deserts getting larger? *Geophys. Res. Lett.* **36**, 1–5 (2009).
12. Bard, E. & Rickaby, R. E. M. Migration of the subtropical front as a modulator of glacial climate. *Nature* **460**, 380–383 (2009).
13. Barker, S. *et al.* Interhemispheric Atlantic seesaw response during the last deglaciation. *Nature* **457**, 1097–1102 (2009).

14. Barker, S. & Diz, P. Timing of the descent into the last Ice Age determined by the bipolar seesaw. *Paleoceanography* **29**, 489–507 (2014).
15. Dyez, K. A., Zahn, R. & Hall, I. R. Multicentennial Agulhas leakage variability and links to North Atlantic climate during the past 80,000-years. *Paleoceanography* **29**, 1238–1248 (2014).
16. Peeters, F. J. C. *et al.* Vigorous exchange between the Indian and Atlantic oceans at the end of the past five glacial periods. *Nature* **430**, 661–665 (2004).
17. Chiessi, C. M., Ulrich, S., Mulitza, S., Pätzold, J. & Wefer, G. Signature of the Brazil-Malvinas Confluence (Argentine Basin) in the isotopic composition of planktonic foraminifera from surface sediments. *Mar. Micropaleontol.* **64**, 52–66 (2007).
18. Hemleben, C., Spindler, M., Breitinger, I. & Deuser, W. G. Field and laboratory studies on the ontogeny and ecology of some globorotaliid species from the Sargasso Sea off Bermuda. *J. Foraminifer. Res.* **15**, 254–272 (1985).
19. Mulitza, S., Dürkoop, A., Hale, W., Wefer, G., & Niebler, H. S. Planktonic foraminifera as recorders of past surface-water stratification. *Geology* **25**, 335–338 (1997).
20. Schiebel, R. & Hemleben, C. Modern planktic foraminifera. *Paläontologische Zeitschrift* **79**, 135–148 (2005).
21. Lohmann, G. P., & Schweitzer, P. N. Globorotalia truncatulinoides' Growth and chemistry as probes of the past thermocline: 1. Shell size. *Paleoceanography* **5**, 55–75 (1990).
22. Kaiser, E. A., Caldwell, A. & Billups, K. North Atlantic Upper-Ocean Hydrography During the Mid-Pleistocene Transition Evidenced by Globorotalia truncatulinoides Coiling Ratios. *Paleoceanogr. Paleoclimatology* **34**, 658–671 (2019).
23. Kucera, M., Rosell-Melé, A., Schneider, R., Waelbroeck, C. & Weinelt, M. Multiproxy approach for the reconstruction of the glacial ocean surface (MARGO). *Quat. Sci. Rev.* **24**, 813–819 (2005).
24. Gottschalk, J., Skinner, L. C. & Waelbroeck, C. Contribution of seasonal sub-Antarctic surface water variability to millennial-scale changes in atmospheric CO<sub>2</sub> over the last deglaciation and Marine Isotope Stage 3. *Earth Planet. Sci. Lett.* **411**, 87–99 (2015).
25. Locarnini, R.A., A.V. Mishonov, O.K. Baranova, T.P. Boyer, M.M. Zweng, H.E. Garcia, J.R. Reagan, D. Seidov, K.W. Weathers, C.R. Paver, and I. V. S. (2019). World Ocean Atlas 2018 , Volume 1 : Temperature NOAA Atlas NESDIS 81 WORLD OCEAN ATLAS 2018 Volume 1: Temperature National Oceanic and Atmospheric Administration. *World Ocean Atlas 2018, Vol. 1 Temp. A. Mishonov, Tech. Ed. NOAA Atlas NESDIS 81, 52pp.* **1**, 52 (2019).
26. Stramma, L. & England, M. On the water masses and mean circulation of the South Atlantic Ocean. *Journal of Geophysical Research: Oceans* **104**, 20863–20883 (1999).
27. Hüls, M., & Zahn, R. Millennial-scale sea surface temperature variability in the western tropical North Atlantic from planktonic foraminiferal census counts. *Paleoceanography* **15**, 659–678 (2000).
28. Jaeschke, A., Rühlemann, C., Arz, H., Heil, G. & Lohmann, G. Coupling of millennial-scale changes in sea surface temperature and precipitation off northeastern Brazil with high-latitude climate shifts during the last glacial period. *Paleoceanography* **22**, 1–10 (2007).
29. Schlitzer, R. Ocean Data View, ODV 5.2. 1. (2020).

30. Bahr, A. *et al.* METEOR-Berichte: South American Hydrological Balance and Paleoceanography during the Late Pleistocene and Holocene (SAMBA) - Cruise No. M125. 96 (2016) doi:10.2312/cr.
31. Campos, M. C. *et al.* A new mechanism for millennial scale positive precipitation anomalies over tropical South America. *Quat. Sci. Rev.* **225**, (2019).
32. Govin, A. *et al.* Terrigenous input off northern South America driven by changes in Amazonian climate and the North Brazil Current retroflection during the last 250 ka. *Clim. Past* **10**, 843–862 (2014).
33. Blaauw, M. & Christeny, J. A. Flexible paleoclimate age-depth models using an autoregressive gamma process. *Bayesian Anal.* **6**, 457–474 (2011).
34. Langner, M. & Mulitza, S. Technical note: PaleoDataView - A software toolbox for the collection, homogenization and visualization of marine proxy data. *Clim. Past* **15**, 2067–2072 (2019).
35. McManus, J. F., Francois, R., Gherardl, J. M., Kelgwin, L. & Drown-Leger, S. Collapse and rapid resumption of Atlantic meridional circulation linked to deglacial climate changes. *Nature* **428**, 834–837 (2004).
36. Lippold, J. *et al.* Does sedimentary  $^{231}\text{Pa}/^{230}\text{Th}$  from the Bermuda Rise monitor past Atlantic Meridional Overturning Circulation? *Geophys. Res. Lett.* **36**, 1–6 (2009).
37. Henry, L. G. *et al.* North Atlantic ocean circulation and abrupt climate change during the last glaciation. *Science (80-. ).* **353**, 470–474 (2016).
38. Campos, M. C. *et al.* Constraining Millennial-Scale Changes in Northern Component Water Ventilation in the Western Tropical South Atlantic. *Paleoceanogr. Paleoclimatology* **35**, 1–32 (2020).
39. Mulitza, S. *et al.* Synchronous and proportional deglacial changes in Atlantic meridional overturning and northeast Brazilian precipitation. *Paleoceanography* **32**, 622–633 (2017).
40. Marshall, J., Donohoe, A., Ferreira, D. & McGee, D. The ocean's role in setting the mean position of the Inter-Tropical Convergence Zone. *Clim. Dyn.* **42**, 1967–1979 (2014).
41. Chiessi, C. M. *et al.* Thermal evolution of the western South Atlantic and the adjacent continent during Termination 1. *Clim. Past* **11**, 915–929 (2015).
42. Chiang, J. C. H. & Friedman, A. R. Extratropical cooling, interhemispheric thermal gradients, and tropical climate change. *Annu. Rev. Earth Planet. Sci.* **40**, 383–412 (2012).
43. McGee, D. *et al.* Hemispherically asymmetric trade wind changes as signatures of past ITCZ shifts. *Quat. Sci. Rev.* **180**, 214–228 (2018).
44. Trenberth, K. E. & Caron, J. M. Estimates of Meridional Atmosphere and Ocean Heat Transports. *J. Clim.* **14**, 3433–3443 (2001).
45. Green, B. & Marshall, J. Coupling of trade winds with ocean circulation damps itcz shifts. *J. Clim.* **30**, 4395–4411 (2017).
46. Portilho-Ramos, R. C. *et al.* Coupling of equatorial Atlantic surface stratification to glacial shifts in the tropical rainbelt. *Sci. Rep.* **7**, (2017).
47. Pedro, J. B. *et al.* Beyond the bipolar seesaw: Toward a process understanding of interhemispheric coupling. *Quat. Sci. Rev.* **192**, 27–46 (2018).

48. Reißig, S., Nürnberg, D., Bahr, A., Poggemann, D. W. & Hoffmann, J. Southward Displacement of the North Atlantic Subtropical Gyre Circulation System During North Atlantic Cold Spells. *Paleoceanogr. Paleoceanography* **34**, 866–885 (2019).
49. Chang, P. *et al.* Oceanic link between abrupt changes in the north Atlantic ocean and the African monsoon. *Nat. Geosci.* **1**, 444–448 (2008).
50. Venancio, I. M. *et al.* Millennial- to Orbital-Scale Responses of Western Equatorial Atlantic Thermocline Depth to Changes in the Trade Wind System Since the Last Interglacial. *Paleoceanogr. Paleoceanography* **33**, 1490–1507 (2018).
51. Rodrigues, R. R., Rothstein, L. M. & Wimbush, M. Seasonal variability of the South Equatorial Current bifurcation in the Atlantic Ocean: A numerical study. *J. Phys. Oceanogr.* **37**, 16–30 (2007).
52. Shemesh, A. *et al.* Sequence of events during the last deglaciation in Southern Ocean sediments and Antarctic ice cores. *Paleoceanography* **17**, 8-1-8-7 (2002).
53. Crosta, X., Sturm, A., Armand, L. & Pichon, J. J. Late Quaternary sea ice history in the Indian sector of the Southern Ocean as recorded by diatom assemblages. *Mar. Micropaleontol.* **50**, 209–223 (2004).
54. Berger, A. & Loutre, M. F. Insolation values for the climate of the last 10 million years. *Quat. Sci. Rev.* **10**, 297–317 (1991).
55. Köhler, P., Nehrbass-Ahles, C., Schmitt, J., Stocker, T. F. & Fischer, H. A 156 kyr smoothed history of the atmospheric greenhouse gases CO<sub>2</sub>, CH<sub>4</sub>, and N<sub>2</sub>O and their radiative forcing. *Earth Syst. Sci. Data* **9**, 363–387 (2017).
56. Stramma, L. The South Indian Ocean Current. *J. Phys. Oceanogr.* **22**, 421–430 (1992).
57. De Deckker, P., Moros, M., Perner, K. & Jansen, E. Influence of the tropics and southern westerlies on glacial interhemispheric asymmetry. *Nat. Geosci.* **5**, 266–269 (2012).
58. Lambert, F., Bigler, M., Steffensen, J. P., Hutterli, M. & Fischer, H. Centennial mineral dust variability in high-resolution ice core data from Dome C, Antarctica. *Clim. Past* **8**, 609–623 (2012).
59. Beal, L. M. *et al.* On the role of the Agulhas system in ocean circulation and climate. *Nature* **472**, 429–436 (2011).
60. Biastoch, A., Böning, C. W., Schwarzkopf, F. U. & Lutjeharms, J. R. E. Increase in Agulhas leakage due to poleward shift of Southern Hemisphere westerlies. *Nature* **462**, 495–498 (2009).
61. Screen, J. A., Gillet, N. P., Stevens, D. P., Marshall, G. J. & Roscoe, H. K. The role of eddies in the Southern Ocean temperature response to the southern annular mode. *J. Clim.* **22**, 806–818 (2009).
62. Jiang, N. & Yan, Q. Evolution of the meridional shift of the subtropical and subpolar westerly jet over the Southern Hemisphere during the past 21,000 years. *Quat. Sci. Rev.* **246**, 106544 (2020).
63. Anderson, R. F. *et al.* Wind-driven upwelling in the southern ocean and the deglacial rise in atmospheric CO<sub>2</sub>. *Science (80-.)* **323**, 1443–1448 (2009).
64. Jaccard, S. L., Galbraith, E. D., Martínez-García, A. & Anderson, R. F. Covariation of deep Southern Ocean oxygenation and atmospheric CO<sub>2</sub> through the last ice age. *Nature* **530**, 207–210 (2016).
65. Levy, R. H., Meyers, S. R., Naish, T. R., Golledge, N. R., McKay, R. M., Crampton, J.

- S., ... Kulhanek, D. K. Antarctic ice-sheet sensitivity to obliquity forcing enhanced through ocean connections. *Nat. Geosci.* **12**, 132–137 (2019).
66. Groeneveld, J. & Chiessi, C. M. Mg/Ca of *Globorotalia inflata* as a recorder of permanent thermocline temperatures in the South Atlantic. *Paleoceanography* **26**, 1–12 (2011).
  67. Howard, W. R., & Prell, W. L. Late Quaternary Surface Circulation of the Southern Indian Ocean and its Relationship to Orbital Variations. *Paleoceanography* **7**, 79–117 (1992).
  68. Stainforth, R. M., Lamb, J. L., Luterbacher, H., Beard, J. H. & Jeffords, R. M. Cenozoic Planktonic Foraminiferal Zonation and Characteristics of Index Formsle. *Univ. Kansas Paleontol. Contrib.* **62**, 1–425 (1975).
  69. Hemleben, C., Spindler, M. & Anderson, O. R. *Modern Planktonic Foraminifera*. (1989).
  70. Volbers, A. N. A. & Henrich, R. Calcium carbonate corrosiveness in the South Atlantic during the Last Glacial Maximum as inferred from changes in the preservation of *Globigerina bulloides*: A proxy to determine deep-water circulation patterns? *Mar. Geol.* **204**, 43–57 (2004).

### **Chapter 3**

#### **3. Millennial-scale negative $\delta^{13}\text{C}$ excursions in the South Atlantic thermocline of the last glacial period**

### **Chapter 4**

#### **4. Concluding remarks and future challenges**

Our set of marine sediment cores allowed the reconstruction of the upper water column conditions at high-resolution during HS for the last 70 kyr. In this dissertation we found out a new proxy for the meridional displacement of the SASG at millennial-scale based on the planktonic foraminifera *Globorotalia truncatulinoides*. According to our findings the large-scale upper column stratification in the South Atlantic was altered by a systematic pattern of meridional shifts in the SASG during HS. Such pattern was responsible transfer of substantial amounts of heat from the SASG to the Southern Ocean, ultimately strengthening deep-water upwelling and CO<sub>2</sub> release to the atmosphere. Therefore, this indicates that the heat stored in the South Atlantic caused by slowdown events in the AMOC (e.g., HS) could have distributed to the Southern Ocean by the SASG, therefore, working in favor of the oceanic bipolar seesaw as well as acting as a positive feedback loop. Noteworthy, this mechanism may have been worked on the same direction in the North Atlantic basin, indicating a striking paleoclimate influence of subtropical gyres. However, the magnitude between decreasing in the strength of the AMOC and its related response in the southward migration of the SASG was unfortunately not feasible to explore in this present dissertation.

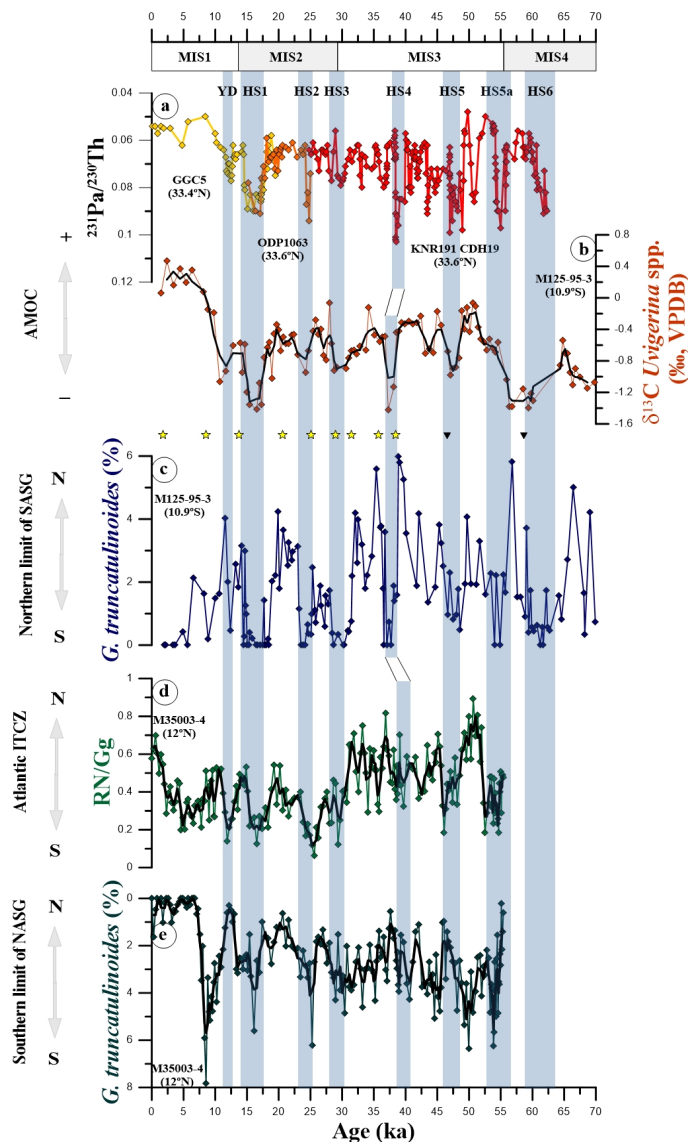
Our high-resolution thermocline-dwelling  $\delta^{13}\text{C}$  records suggest that the SACW is influenced by different water masses. Our indications point toward the presence of Agulhas leakage thermocline waters predominantly in the NW-South Atlantic region. Under a reduced strength of the AMOC the thermocline circulation had its residence

time increased, which possibly increased the amount of respired carbon accumulation in agreement to our magnitudes of negative  $\delta^{13}\text{C}$  excursions observed during HS. In general, the negative  $\delta^{13}\text{C}$  excursions in the thermocline waters were driven by the strengthening of upwelling and an inefficient biological pump in the Southern Ocean. Remarkably, this oceanic pathway represents the upper branch of the AMOC connecting Indian and Atlantic oceans. Future studies should investigate in depth the role of Indian Ocean thermocline waters in the tropical South Atlantic during past abrupt millennial-scale climate changes. By contrast, we suggest that the SACW in southern Brazilian margin was sourced by central and intermediate water masses mixed at the BMC, which is characterized by a lighter type of subtropical mode water. These evidences reveal a stratified SACW-shaped by different water layers and geochemical proprieties in the southern Brazilian margin during HS.

## Chapter 5

### 5. Appendix 1 – Supplementary material to chapter 2

**Figure S5.1:**



## Supplementary Figure Caption

**Figure S5.1.** Relationship between the Atlantic Intertropical Convergence Zone and northern limit of the South Atlantic Subtropical Gyre (nSASG). (a) Bermuda Rise  $^{231}\text{Pa}/^{230}\text{Th}^{1-3}$ ; (b)  $\delta^{13}\text{C}$  *Uvigerina* spp. from the study site<sup>4</sup>; (c) Relative abundance of *Globorotalia truncatulinoides* from core M125-95-3; (d)  $\% \text{Neogloboquadrina}/(\% \text{Neogloboquadrina} + \% \text{G. glutinata})$  (RN/Gg) ratio as a proxy for the position of the Atlantic ITCZ in the Tobago Basin core M35003-4<sup>5</sup>; (e) Relative abundance of *Globorotalia truncatulinoides* from core M35003-4 (Tobago Basin)<sup>6</sup>. Yellow stars on top of panel “c” depict calibrated radiocarbon ages and black triangles depict tie-points used to produce the age model of core M125-95-3 ( $2\sigma$  standard error smaller than symbol size)<sup>7</sup>. Blue vertical bars represent millennial-scale Heinrich Stadials (HS) 6-1 and the Younger Dryas (YD). Marine Isotope Stages (MIS) are depicted below the upper horizontal axis. Atlantic Meridional Overturning Circulation (AMOC), Intertropical Convergence Zone (ITCZ), North Atlantic Subtropical Gyre (NASG), South Atlantic Subtropical Gyre (SASG).

### 5.1 Supplementary references

1. McManus, J. F., Francois, R., Gherardl, J. M., Kelgwin, L. & Drown-Leger, S. Collapse and rapid resumption of Atlantic meridional circulation linked to deglacial climate changes. *Nature* **428**, 834–837 (2004).
2. Lippold, J. *et al.* Does sedimentary  $^{231}\text{Pa}/^{230}\text{Th}$  from the Bermuda Rise monitor past Atlantic Meridional Overturning Circulation? *Geophys. Res. Lett.* **36**, 1–6 (2009).
3. Henry, L. G. *et al.* North Atlantic ocean circulation and abrupt climate change during the last glaciation. *Science (80-.)* **353**, 470–474 (2016).
4. Campos, M. C. *et al.* Constraining Millennial-Scale Changes in Northern Component Water Ventilation in the Western Tropical South Atlantic. *Paleoceanogr. Paleoclimatology* **35**, 1–32 (2020).
5. Portilho-Ramos, R. C. *et al.* Coupling of equatorial Atlantic surface stratification to glacial shifts in the tropical rainbelt. *Sci. Rep.* **7**, (2017).
6. Hüls, M., & Zahn, R. Millennial-scale sea surface temperature variability in the western tropical North Atlantic from planktonic foraminiferal census counts. *Paleoceanography* **15**, 659–678 (2000).
7. Campos, M. C. *et al.* A new mechanism for millennial scale positive precipitation anomalies over tropical South America. *Quat. Sci. Rev.* **225**, (2019).